




RESEARCH ARTICLE

WILEY

Controlling effects of pore-throat structure and fractal characteristics on the physical properties of ultra-low permeability sandstone reservoirs: A case study of the sixth member of the Yanchang Formation in the Xiaojiahe area, Ordos Basin

Guoxiong Li^{1,2}  | Chenglin Liu^{1,2}  | Ya-nan Zhou³ | Hanning Wu³ |
Rizwan Sarwar Awan^{1,2}  | Fei Shi⁴ | Yunfei Wu^{1,2} | Qibiao Zang^{1,2} |
Yuping Wu^{1,2}

¹State Key Laboratory of Petroleum Resources and Prospecting, China University of Petroleum, Beijing, People's Republic of China

²College of Geosciences, China University of Petroleum, Beijing, People's Republic of China

³Department of Geology, Northwest University, Xi'an, People's Republic of China

⁴Yanchang Oilfield Co., Ltd. Zichang Oil Production Plant, Zichang, People's Republic of China

Correspondence

Chenglin Liu, State Key Laboratory of Petroleum Resources and Prospecting, China University of Petroleum, Beijing 102249, People's Republic of China.
Email: lclzgx@126.com

Funding information

Key Technologies Research and Development Program, Grant/Award Number: 41872127; National Natural Science Foundation of China, Grant/Award Number: 2021YFA0719000

Handling Editor: Y. Jang

Low and ultra-low permeability reservoirs are widely developed in the Upper Triassic Yanchang Formation in the Ordos Basin, and its intricate pore throat structure has a significant impact on the physical properties and heterogeneity of reservoirs. This paper conducted a series of experiments to investigate the petrology, pore structure, fractal characteristics of ultra-low permeability sandstone reservoirs, and influencing factors of the physical properties. The results show the sixth member of the Yanchang Formation (Chang 6) reservoir in the Xiaojiahe area is dominated by feldspathic sandstone. The main pores are intergranular pores, followed by dissolution pores. The Chang 6 sandstone has been categorized into four types (type I–IV) based on the traits of mercury intrusion curves. The high content of quartz and feldspar in the detrital components is conducive to improving the physical properties of the reservoir. The pore-throat structure parameters, such as displacement pressure, median pressure, and pore throat radius can characterize the change in physical properties and reservoir quality. According to the capillary pressure fractal model of r_{apex} (Pittman's plot apex radius), demonstrating the ultra-low permeability, sandstone has a binary structure. The fractal dimensions D_2 and D_p are more appropriate for characterizing the heterogeneity of the pore structure. The effects of different pore-throat size scales on the physical properties of the reservoir have a discrepancy. Relatively large pore throats ($r > r_{\text{apex}}$), non-nanoscale pore throats ($\text{Por}_{r>0.1}$), and effective movable pore throats (Por_{em}) have significantly positive control effects on permeability and reservoir quality. In contrast, the development of nanoscale pore throats ($\text{Por}_{r<0.1}$) and micropore throats of failure to enter mercury (Por_{fem}) are unfavourable to reservoir performance. In conclusion, combining detrital components, pore-throat structure, fractal characteristics, and other factors controlled the reservoir quality of ultra-low permeability sandstone.

KEYWORDS

fractal characteristics, Ordos Basin, pore-throat structure, ultra-low permeability reservoir, Yanchang Formation

1 | INTRODUCTION

Ultra-low permeability sandstone is a crucial unconventional oil and gas reservoir widely developed around the globe. In China, the sixth member of the Yanchang Formation (Chang 6) in the Ordos Basin is considered an ultra-low permeability sandstone reservoir (Zhu et al., 2016; Zou et al., 2014). The average permeability of reservoirs is only 0.1 ~ 1 mD. These reservoirs are usually characterized by fine-grained sediments, poor physical properties, large seepage resistance, large diagenetic differences, strong heterogeneity, micro-fractures development, and stable reservoir distribution (Nelson, 2009; Pittman, 1992; Wang et al., 2017; Wang, Chi, et al., 2018; Wang, Jiao, et al., 2018), and 73.7% of the proven oil reserves are chiefly distributed in such reservoirs (Guo et al., 2012).

Ultra-low permeability reservoirs have a wide distribution range of pore throats and a complex pore system. The pore structure and pore throat connectivity have an essential impact on seepage capacity and reservoir productivity distribution (Wang, Luo, Lei, Zhang, et al., 2020; Zang et al., 2022). Therefore, studying reservoir microscopic pore structure and heterogeneity is vital for evaluating the reservoir quality and the exploration potential of oil and gas reservoirs. Reservoir geologists generally study the pore structure of sandstone through the high-pressure mercury intrusion (HPMI) test and nuclear magnetic resonance (NMR) to obtain parameters, such as pore throat size, uniformity, and connectivity (Huang et al., 2020; Wu et al., 2022). The relationship between pore throat characteristic parameters and reservoir porosity and permeability can be used to reflect better the dominant factors of reservoir storage and permeability (Lai, Wang, Cao, et al., 2018; Lai, Wang, Wang, et al., 2018; Wang, Chi, et al., 2018; Wang, Jiao, et al., 2018; Zhao, Wu, & Wu, 2007). Pore-throat size is a critical factor in evaluating reservoir quality, and different pore throat levels diversely control the physical properties (Lai & Wang, 2015; Nabawy et al., 2009; Nelson, 2009). Previous studies have shown that pore throat size significantly influences reservoir permeability (Lai, Wang, Cao, et al., 2018; Rezaee et al., 2012). The large pore throat contributed more than 80% to permeability and was the main factor of permeability change (Liu et al., 2020; Wang, Luo, Lei, Zhang, et al., 2020; Zhu et al., 2019).

Since the fractal theory was introduced into the field of petroleum geology, it has been frequently employed to describe the pore structures and assesses the petrophysical properties of sedimentary rocks (Hao et al., 2017; Huang et al., 2018; Mandelbrot, 1982; Wang et al., 2022). Numerous researchers have used scanning electron microscope (SEM) (Katz & Thompson, 1985), microscopic thin sections (Hansen & Skjeltorp, 1988), HPMI (Angulo et al., 1992; Dou et al., 2021; Li, 2010; Su et al., 2018), and other methods to study the fractal characteristics of the pore structure. The fractal dimension is acquired based on the self-similarity of reservoir micro-pores for quantitatively evaluating reservoir heterogeneity and complexity (Wang et al., 2019; Wang, Chi, et al., 2018; Wang, Jiao, et al., 2018). The HPMI method characterizes the fractal properties of porous materials, mainly including water saturation (wetting phase) and mercury saturation method (non-wetting phase). It is considered that the

mercury saturation method is more appropriate for characterizing the heterogeneity of ultra-low permeability sandstone (Wang et al., 2019; Wang, Chi, et al., 2018; Wang, Jiao, et al., 2018; Wang, Wu, Li, & Guo, 2020).

Although predecessors have made an amount of meaningful research on the physical properties of ultra-low permeability reservoirs, many pore-throat parameters obtained by mercury injection experiments can effectively characterize the reservoir's pore structure from different aspects (Dou et al., 2021; Lai, Wang, Cao, et al., 2018; Wang, Chi, et al., 2018; Wang, Jiao, et al., 2018). However, the research on the controlling effect of pore throat size on physical properties and the pore throat parameters related to reservoir permeability is relatively weak. Based on the current research situation, this paper takes the Chang 6 sandstone reservoir in the Xiaojiahe area as the research object. Given the problems of poor physical properties and rapid oil layer change of the sandstone reservoir. The petrology, physical properties, and pore structure of the Chang 6 reservoir in the study area are analysed by employing physical property tests, thin section identification, SEM observation, and mercury injection. On this basis, we discuss the controlling factors of reservoir physical properties, refine the microscopic pore throat structure, and clarify the impact of various pore throat spaces on permeability to provide a reference for evaluating reservoir quality.

2 | GEOLOGICAL SETTINGS

The Xiaojiahe area in the Ordos Basin is located on the eastern part of the Yishan slope, with an area of about 45 km² (Figure 1a). The structure is relatively simple, and the elevation difference between the eastern and western structures is about 90 m. Overall, the structure is a gentle west-dipping monocline with a slope angle of about 0.5 degrees, and the slope gradient is 8 ~ 10 m per km. The structural traps are not developed in the study area. However, low-amplitude nasal structures trending nearly east-west are locally developed through differential compaction and have a certain controlling effect on the enrichment of hydrocarbons. The study area belongs to the northeastern sedimentary system. The sedimentary provenance direction is mainly from the northeast direction, and the parent rock area is mainly the northern Yinshan ancient continent and the Daqingshan area (Liu et al., 2007; Zhao, Luo, et al., 2007). The bottom to the top of the Yanchang Formation is classified into 10 oil-bearing members (Chang 10 ~ Chang 1) and its sedimentary evolution recorded the whole formation, development, and disappearance process of the large continental lake basin (Li et al., 2009). The sedimentary period of Chang 6 in the study area belonged to the peak period of lake delta construction and developed delta plain subfacies. The reservoirs are mainly distributed in microfacies, such as distributary channels and natural levees. The buried depth of the Chang 6 Formation in this area is shallow, with an average of 650 m ~ 780 m, and the thickness of the formation is about 130 m. It can be divided into four oil layers (Chang 6₁ ~ Chang 6₄) and several small layers (Figure 1b) that are important reservoirs.

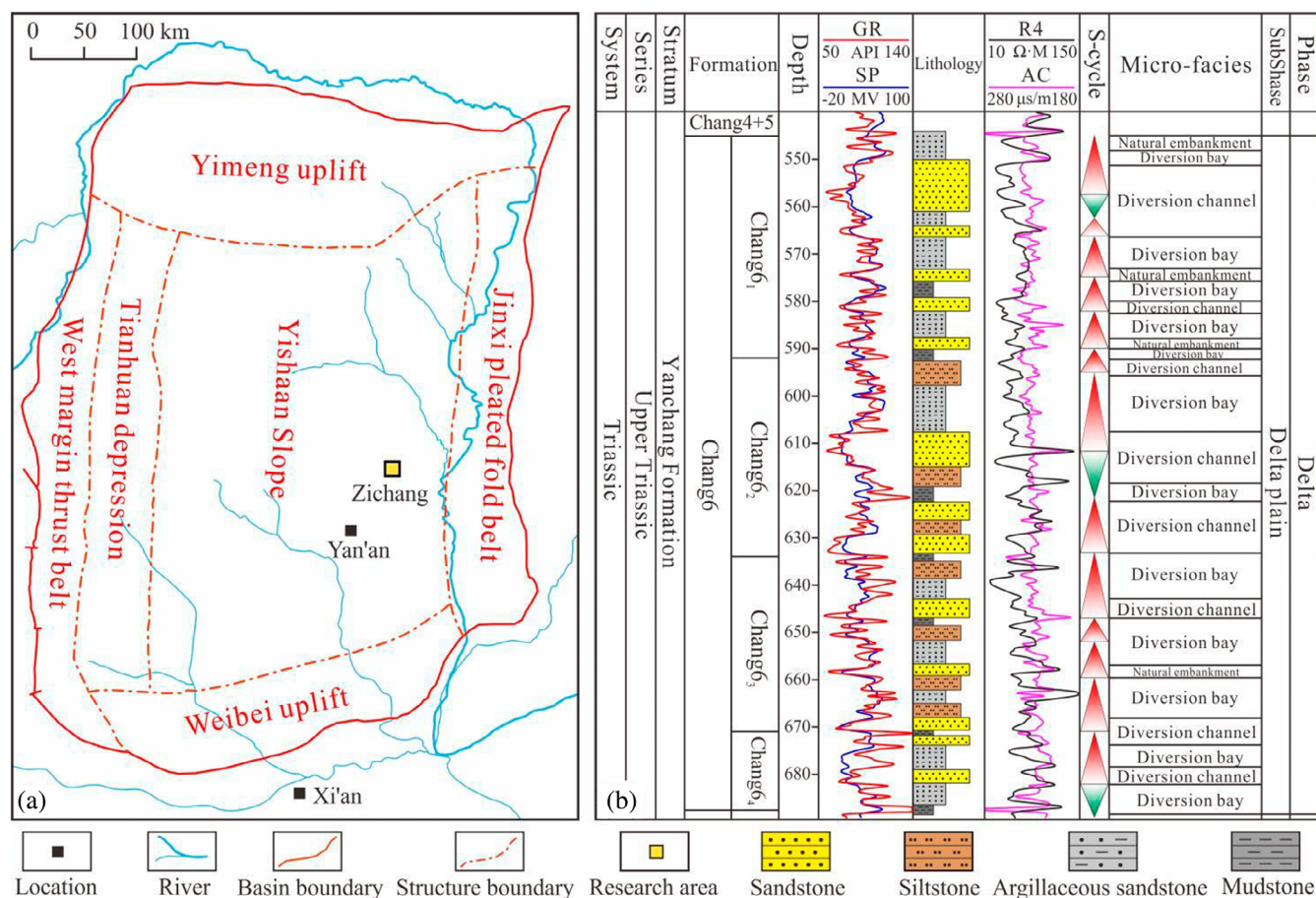


FIGURE 1 (a) Showing location of the research area and the structural units; (b) Stratigraphic column of the sixth member of the Yanchang Formation in the Xiaojiahe area.

3 | DATABASE AND METHODS

3.1 | Experimental samples and preparation methods

This research utilized the ultra-low permeability well-core samples of Chang 6 from the Xiaojiahe area of the Ordos Basin for detailed analysis. The diameter of the drill core samples is 2.54 cm, with a length of about 5.00 ~ 8.00 cm in the plunger-shaped core. Prior to analysis, each sample is cleaned with an alcohol and chloroform solution for 2 weeks to get rid of any residual oil in the sandstone and then dried in a vacuum for 24 h at 110°C. These samples are further used to thin section examination, SEM, HPMT, and physical property test analysis.

The processed samples are used to prepare thin sections by vacuum, and blue epoxy resin impregnation is utilized for pore and throat characterization. A polarizing microscope is employed for optical observations. The petrology and pore statistical analysis were carried out by the point-counting method to determine the pore type and face rate. The gold-coated samples are used for SEM to observe the size, morphology, and symbiotic relationship of different authigenic minerals (especially clay minerals) under the FEI Quanta 200F SEM.

The helium porosimeter is employed to measure the porosity of the formation through well-cores. However, the permeability is tested by the core plunger pressure drop method, which is suitable for a permeability range of 0.001–30,000 mD. The HPMT experiment is carried out using an AutoPore IV mercury intrusion metre. The experimental conditions were room temperature 20°C, and mercury interfacial tension of 0.49 N/m. In addition, the Research Institute of Zichang Oil Production Plant also provided a lot of test and analysis data, including experimental data such as thin section identification, mineral composition analysis, porosity, and permeability measurement, a reliable basis for this study.

3.2 | Fractal theory

A French mathematician Mandelbrot initially proposed the fractal theory to describe the structural traits of complex objects in nature (Mandelbrot, 1975). Subsequently, many researchers used fractal geometry theory to deduce the calculation formula of the fractal dimension. Suppose the pore structure of the reservoir has fractal properties. In that case, there is a significant linear correlation between $\lg S_{Hg}$ and $\lg P_c$ (or $\lg R_p$), and can determine the fractal

dimension from the coefficients of the linear regression equation. It can more accurately capture the heterogeneous characteristics of complex pore structures.

This study calculated the fractal dimension of the pore throat using the mercury injection test data of 18 sandstone samples. The relationship between the number of pores $N(r)$ greater than the radius r in the sandstone sample and the radius r can be described as (Mandelbrot, 1982):

$$N(r) \propto r^{-D}, \quad (1)$$

where D is the fractal dimension, \propto means 'proportional to'.

In the capillary model, assuming rock pores are composed of capillary bundles, the number of pores $N(r)$ can calculate as (Li, 2010):

$$N(r) = \frac{V_{Hg}(r)}{\pi r^2 l}, \quad (2)$$

where $V_{Hg}(r)$ is the cumulative mercury volume when the pore radius is r , and l is the length of the capillary.

Equations (3) and (4) can be acquired by combining Equations (1) and (2).

$$\frac{V_{Hg}(r)}{\pi r^2 l} \propto r^{-D}, \quad (3)$$

$$V_{Hg}(r) \propto r^{2-D} \quad (4)$$

According to the capillary pressure calculation formula (Washburn, 1921), the pore radius r and the capillary pressure can be converted and calculated:

$$P_c = \frac{2\sigma \cos \theta}{r}, \quad (5)$$

where P_c is the capillary pressure (MPa); σ is the surface tension between mercury and air (N/m); θ is the contact angle between mercury and rock ($^\circ$).

Equation (5) can be substituted into Equation (4) to produce Equation (6):

$$V_{Hg}(r) \propto P_c^{-(2-D)} \quad (6)$$

Defined by the mercury saturation (S_{Hg}) in the rock sample, the $V_{Hg}(r)$ can be replaced by the S_{Hg} , then Equation (6) is converted into:

$$S_{Hg} = \alpha P_c^{-(2-D)}, \quad (7)$$

where α is a constant. Equation (7) indicates that under the double-logarithmic coordinate of $\lg(S_{Hg}) - \lg(P_c)$ if the trend line is straight, the fractal dimension can be obtained by the slope k of the straight line as $D = k + 2$.

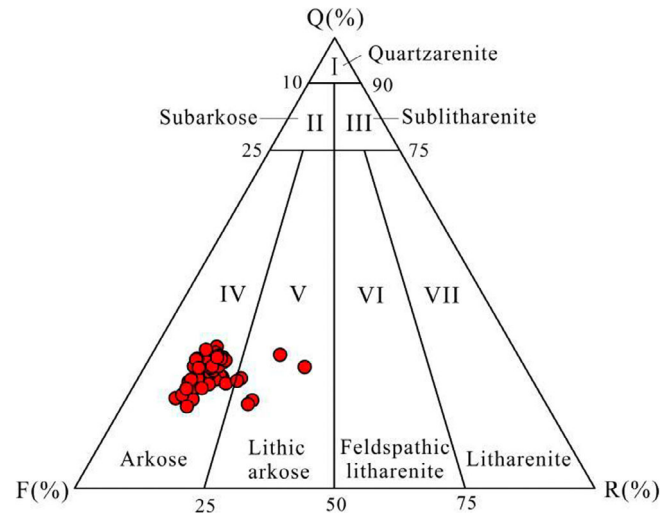


FIGURE 2 Classification of the Chang 6 sandstone in the Xiaojiache area (range from Folk et al., 1970).

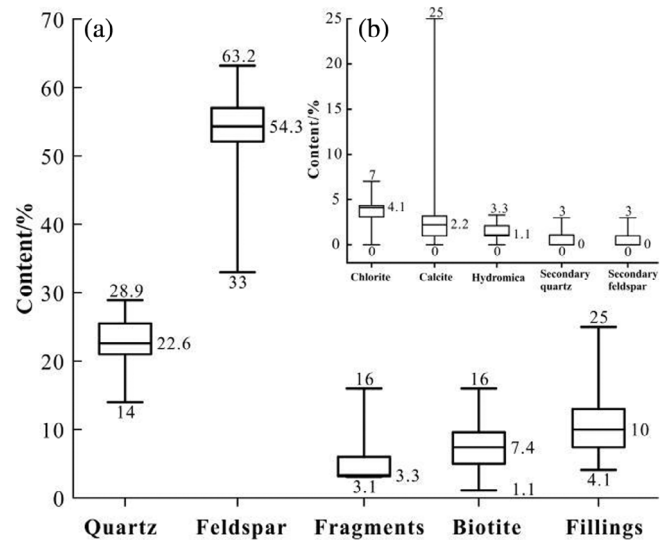


FIGURE 3 Mineral composition of the Chang 6 sandstone.

4 | RESULTS

4.1 | Reservoir petrophysical properties

4.1.1 | Petrology characteristics

The ternary plot between quartz, feldspar, and rock fragments (Figure 2: Q-F-R) exhibits that the Chang 6 sandstone in the Xiaojiache area is mainly composed of feldspar sandstone, followed by lithic feldspar sandstone (Folk et al., 1970). The quartz content in the sandstone reservoir ranges from 14.0% to 28.9%, with an average of 22.8%. The feldspar content varies from 33.0% to 63.2%, with a mean of 53.8%. In feldspar, potassium feldspar accounts for 34.9%, while plagioclase accounts for 18.97%. The biotite content fluctuates amongst 1.1%

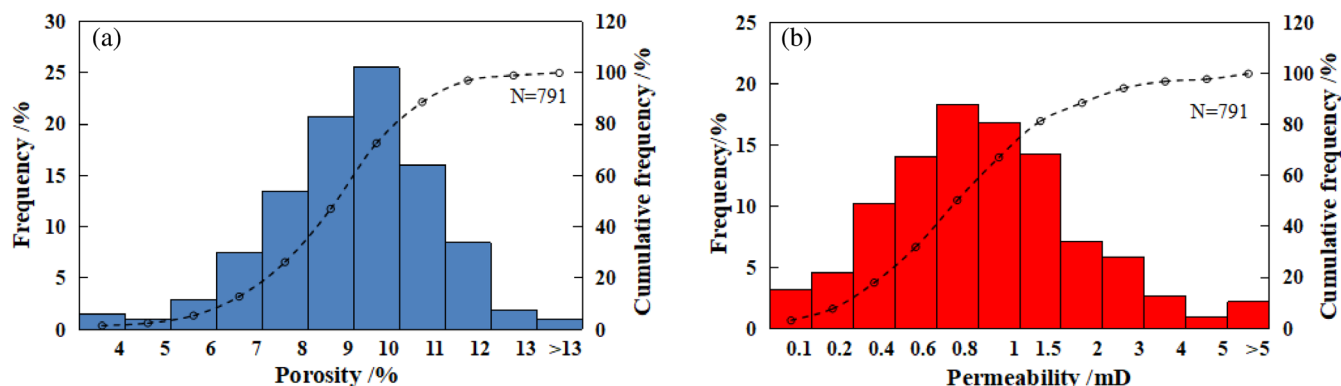


FIGURE 4 Frequency distribution of porosity (a) and permeability (b).

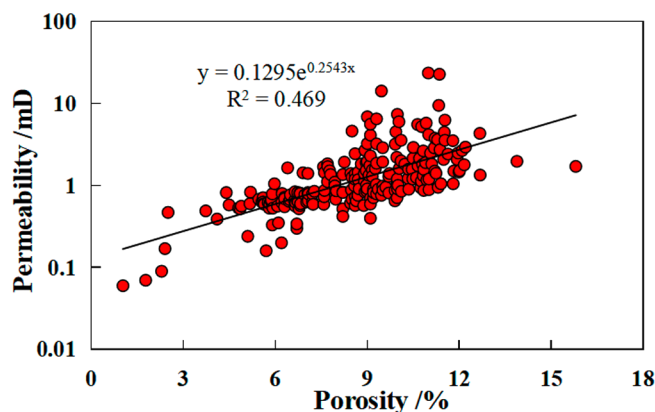


FIGURE 5 Relationship between porosity and permeability.

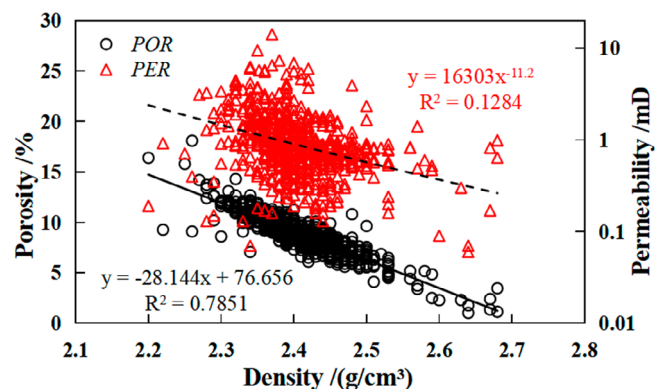


FIGURE 6 Relationship between density and physical properties of sandstone.

and 16.0%, with an average of 7.3%. The debris content is between 3.1% and 16.0%, averaging 5.1%. The debris mainly consists of sedimentary rock debris, metamorphic rock debris, and less magmatic rock debris. The interstitial content is between 4.1% and 25%, with an average of 11.02%, mainly including heterobases and cement. The content of chlorite and calcite is the highest, chlorite content is 0% ~ 7.0%, with a mean of 3.37%, calcite content is 0% ~ 25.0%, averaging 3.24%, followed by hydromica with a content of 1.25% (Figure 3). In

addition, there are minimal amounts of illite, kaolinite, turbidite, and pyrite cement.

4.1.2 | Porosity and permeability

The petrophysical properties of 791 samples show the porosity of the Chang 6 sandstone is between 1.03% and 19.45%, with a mean of 8.95%. More precisely, the porosity mainly varies in the range of 7% ~ 11%, accounting for 75.73% of the samples (Figure 4a). The permeability is amongst 0.02 ~ 14.19 mD, averaging 1.14 mD. However, the main permeability distribution range is 0.2 ~ 1.5 mD, accounting for 73.7% of the specimens (Figure 4b). According to industry standards (SY/T 6285-2011), the Chang 6 reservoir has mostly low and ultra-low porosity and ultra-low permeability. The crossplot demonstrates the relationship between sandstone's permeability and porosity, but $R^2 = 0.469$ and the correlation are relatively weak, indicating the development of porosity controls the permeability change up to a certain extent (Figure 5). Still, the evolution of porosity and permeability is a complex process, and the microscopic pore-throat structure significantly impacts permeability (Lai, Wang, Wang, et al., 2018; Zhao, Wu, & Wu, 2007). The bivariate graph between porosity and density deciphers that sandstone density negatively correlates with porosity ($R^2 = 0.7851$; Figure 6). In contrast, it has a poor correlation with permeability ($R^2 = 0.1284$; Figure 6). Indicating the variation of sandstone porosity, which is closely related to the density, but has little effect on the permeability. In other words, larger porosity does not necessarily possess better permeability. Reflecting ultra-low permeability sandstones have strong heterogeneity, and the controlling factors of permeability are relatively complex.

Reservoir quality index (RQI) and flow zone indicator (FZI) have been widely used to characterize reservoirs with similar pore-throat geometrical attributes (hydraulic units). And their expression equations are as Equations (8) and (9) (Amaefule et al., 1993). The larger the RQI and FZI values in sandstone, the better the reservoir quality and physical properties. The results of Chang 6 sandstone samples present a RQI ranges from 0.015 to 0.151 with an average of 0.082, and FZI varies between 0.16 and 1.23, averaging 0.73 (Table 1).

TABLE 1 Pore-throat structure parameters of the Chang 6 sandstone reservoir in the Xiaojiahe area.

Type	Samples	Φ (%)	K (mD)	RQI	FZI	P_d (MPa)	P_{50} (MPa)	R_{max} (μm)	R_a (μm)	R_{50} (μm)	S_p	S_{kp}	τ	S_{Hgmax} (%)	W_E (%)
I	S1	10.9	2.52	0.151	1.23	0.31	3.00	2.41	0.52	0.25	0.47	1.66	1.88	81.20	38.92
	S2	11.2	2.01	0.133	1.05	0.26	2.98	2.90	0.50	0.25	0.49	2.19	2.12	81.18	35.76
	S3	10.7	1.57	0.120	1.00	0.21	1.71	3.63	0.80	0.44	0.64	1.57	3.50	78.38	35.24
	S4	11.2	1.41	0.111	0.88	0.2	3.14	3.73	0.75	0.24	0.62	1.88	3.47	78.21	38.59
II	S5	10.4	0.75	0.084	0.73	0.95	6.97	0.79	0.19	0.11	0.14	2.33	1.04	69.20	39.83
	S6	10.9	0.84	0.087	0.71	0.43	5.02	1.76	0.40	0.15	0.34	1.95	2.33	73.52	38.78
	S7	10.1	1.14	0.105	0.94	0.69	7.09	1.08	0.28	0.11	0.20	1.83	1.23	68.19	44.65
	S8	10.4	0.67	0.080	0.69	0.78	6.68	0.96	0.26	0.11	0.18	1.81	1.50	72.24	41.63
	S9	10.9	0.80	0.085	0.70	0.48	4.13	1.57	0.32	0.18	0.27	2.18	1.93	76.21	36.96
	S10	9.6	0.98	0.100	0.94	0.52	4.69	1.45	0.35	0.16	0.26	1.82	1.69	72.38	38.43
	S11	8.8	0.75	0.092	0.95	0.74	5.70	1.00	0.23	0.13	0.17	2.00	1.22	71.92	35.51
	S12	9.4	1.06	0.105	1.02	0.67	4.49	1.12	0.28	0.17	0.21	1.73	1.28	76.26	35.65
III	S13	8.7	0.41	0.068	0.72	1.56	14.62	0.48	0.12	0.05	0.08	2.42	0.77	63.08	42.65
	S14	8.9	0.24	0.052	0.53	1.90	13.35	0.40	0.10	0.06	0.07	2.23	0.86	67.11	39.33
	S15	10.5	0.21	0.044	0.38	1.62	11.85	0.46	0.13	0.06	0.08	2.21	1.24	62.74	26.02
IV	S16	8.3	0.06	0.027	0.29	3.84	22.00	0.20	0.06	0.03	0.03	2.31	0.91	58.73	40.50
	S17	8.7	0.02	0.015	0.16	5.87	31.05	0.13	0.04	0.02	0.02	2.39	0.81	50.96	33.60
	S18	7.4	0.04	0.023	0.29	5.45	25.26	0.14	0.05	0.03	0.02	2.2	0.79	54.20	39.30

Abbreviations: FZI, flow zone indicator; K , permeability; P_{50} , median saturation pressure; P_d , threshold pressure; R_{50} , median radius; R_a , average pore-throat radius; R_{max} , maximum pore-throat radius; RQI, reservoir quality index; S_{Hgmax} , maximum mercury saturation; S_{kp} , skewness factor; S_p , sorting factor; W_E , efficiency of mercury withdrawal; τ , mercury injection tortuosity; Φ , porosity.

$$RQI = 0.0314 \sqrt{\frac{K}{\varphi}} \quad (8)$$

$$FZI = 0.0314 \left(\frac{1-\varphi}{\varphi} \right) \sqrt{\frac{K}{\varphi}} \quad (9)$$

4.2 | Pore-throat types

The optical analysis of the studied sandstone samples using thin sections and SEM exhibited various types of pores in the Chang 6 reservoir. It mainly comprises intergranular pores, followed by dissolution pores. However, intercrystalline micropores and a few microfractures are formed in the region. Intergranular pores account for 53.5%, dissolution pores for 32.8%, intercrystalline micropores for 9.1%, microcracks for 4.6%, and the average face rate is 6.8%.

The intergranular pores are mainly complete and residual intergranular pores. The complete intergranular pores are formed pore space by mutual brace between grains and are not filled or dissolved (Figure 7a). Some detrital grains or diagenesis minerals are filled in the residual intergranular pores. Consequently, pore space became smaller. For example, in the early stage of diagenesis, chlorite is distributed in the sandstone pores in the form of a dispersion or thin film (Figure 7b); the pores and throats still have a good reservoir and percolation capacity. However, the middle and late stages of chlorite have a high degree of eumorphism, and the aggregation forms are

mostly needle-like, laminar-like, or fluffy spherical (Figure 7c). These chlorites are concentrated and filled into pores to reduce reservoir space. Some carbonate cement (Figure 7d) and quartz secondary enlargement cement (Figure 7e) also filled the intergranular pores, making the space further smaller and the reservoir's physical properties worse. The dissolution pores include granular dissolution pores, such as feldspar and rock debris, forming strip, grid, or honeycomb dissolution pores in the grains (Figure 7f). If the dissolution effect is too strong, mould pores will develop or connect with intergranular dissolution pores. It can effectively promote the connectivity between pores and throats. Intercrystalline micropores are a part of the microscopic space of mineral components. It is developed in the intercrystalline cement or residual intergranular pore fillings, with pore diameters of about 5 μm , showing cluster shape and poor connectivity (Figure 7g). Micro-fractures are usually formed by brittle grains, such as feldspar and quartz that rupture under diagenetic changes or mechanical stresses. These micro-fractures usually extend to a narrow and long fracture (Figure 7h), which can improve the local permeability and connectivity of the reservoir. The types of throat are mainly curved sheets and necking (Figure 7i).

4.3 | Pore-throat structure characteristics

The HPMT test is a common method to study the pore structure of sandstone reservoirs (Li, 2010; Nabawy et al., 2009). According to the

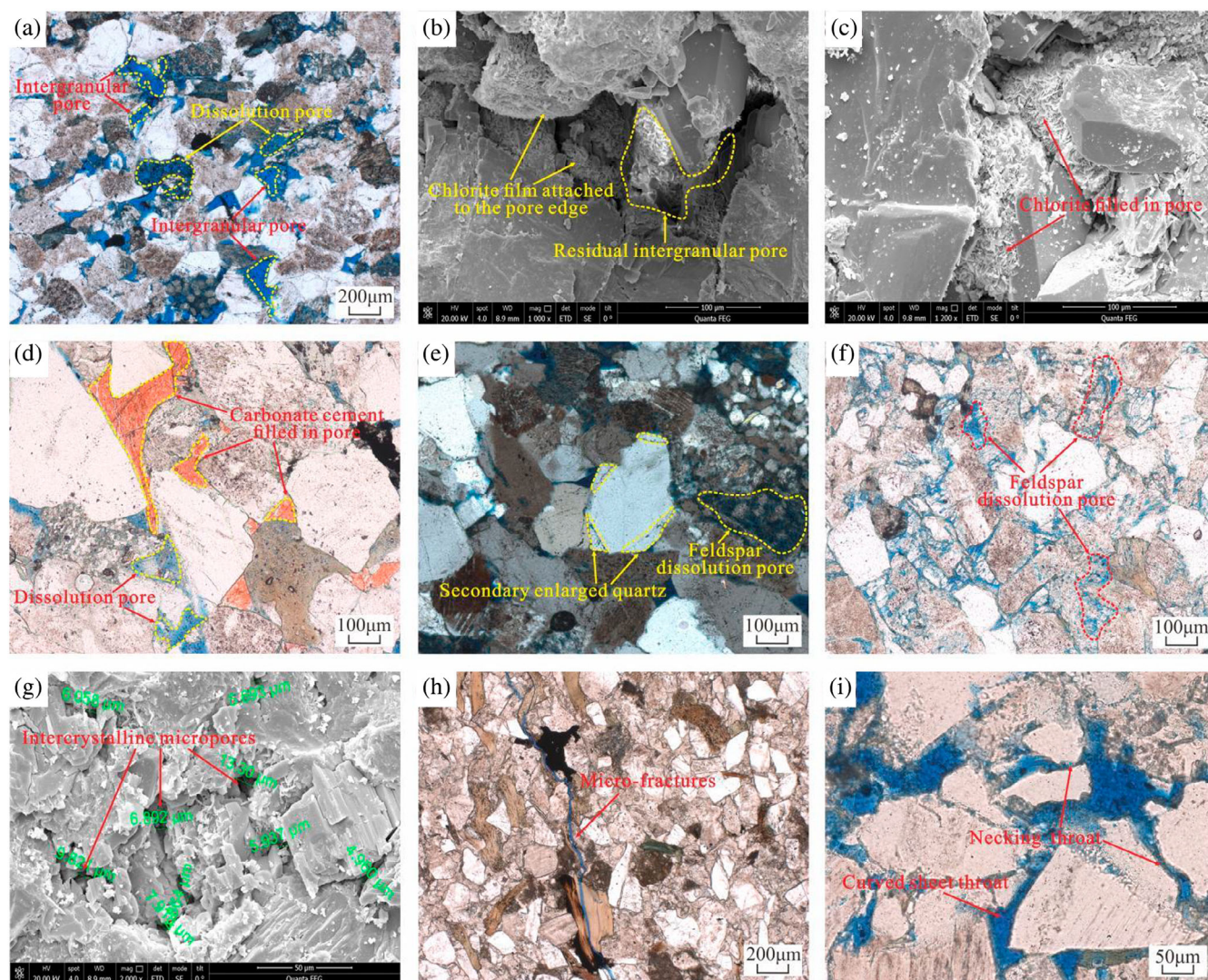


FIGURE 7 Showing the pore throat types in thin section and SEM images. (a) ZT3516, 572.55 m, intergranular pores; (b) ZT3071, 653.45 m, chlorite film attached to the pore edge; (c) ZT3516, 577.55 m, chlorite filled pores; (d) ZT1139, 614.45 m, carbonate cement filled in pore; (e) ZT3516, 572.03 m, secondary enlarged quartz; (f) ZT1139, 645.99 m, feldspar dissolution pores; (g) ZT1139, 614.85 m, intercrystalline micropores; (h) ZT1139, 631.66 m, micro-fractures; (i) ZT3071, 653.45 m, curved sheet throat and necking throat.

Washburn equation (1921), the change in mercury injection saturation is correspondingly transformed into the size of pore throats. Therefore, the mercury intrusion curve can better reflect the microscopic pore structure of the reservoir (Lai, Wang, Cao, et al., 2018; Wang, Chi, et al., 2018; Wang, Jiao, et al., 2018). The HPMI results of the studied Chang 6 sandstone samples of the study area decipher good throat distribution uniformity, moderate sorting, low mercury withdrawal efficiency, general connectivity, and significant differences in threshold pressure and throat radius (Figure 8). The capillary pressure curves of Chang 6 sandstone can be categorized into four types based on the mercury injection parameters, the physical properties, and the shape of the mercury injection curve (Table 1). Each capillary pressure curve corresponded to a specific range of physical parameters and pore throat structure parameters. From type I to type IV sandstone, the threshold pressure steadily increased, while the maximum mercury injection saturation gradually decreased. However, the pore throat

size distribution interval narrowed slowly, and the permeability significantly reduced with the decrease of the pore throat radius (Table 1).

The mercury injection curve of the type I sample appeared to be relatively wide and gentle in the early stage, with a low position (Figure 8a₁). The threshold pressure is minor, generally less than 0.40 MPa, with an average of 0.25 MPa. The median pressure is less than 4.0 MPa, with a mean of 2.71 MPa. The maximum pore throat radius is greater than 2.40 μm , and the average pore throat radius is between 0.5 and 0.8 μm , averaging 0.64 μm . The average sorting coefficient is 0.56, with medium sorting. The reservoir has good physical properties, with the porosity generally larger than 10% and the permeability typically greater than 1.0 mD. The type I sample pore throat size exhibits a single peak and has the widest size distribution range, spanning from 0.016 to 4.0 μm . The distribution of the large throat (0.4 ~ 2.5 μm) displays a single peak of positive skewness with slightly coarse distortion, and the distribution frequency accounted

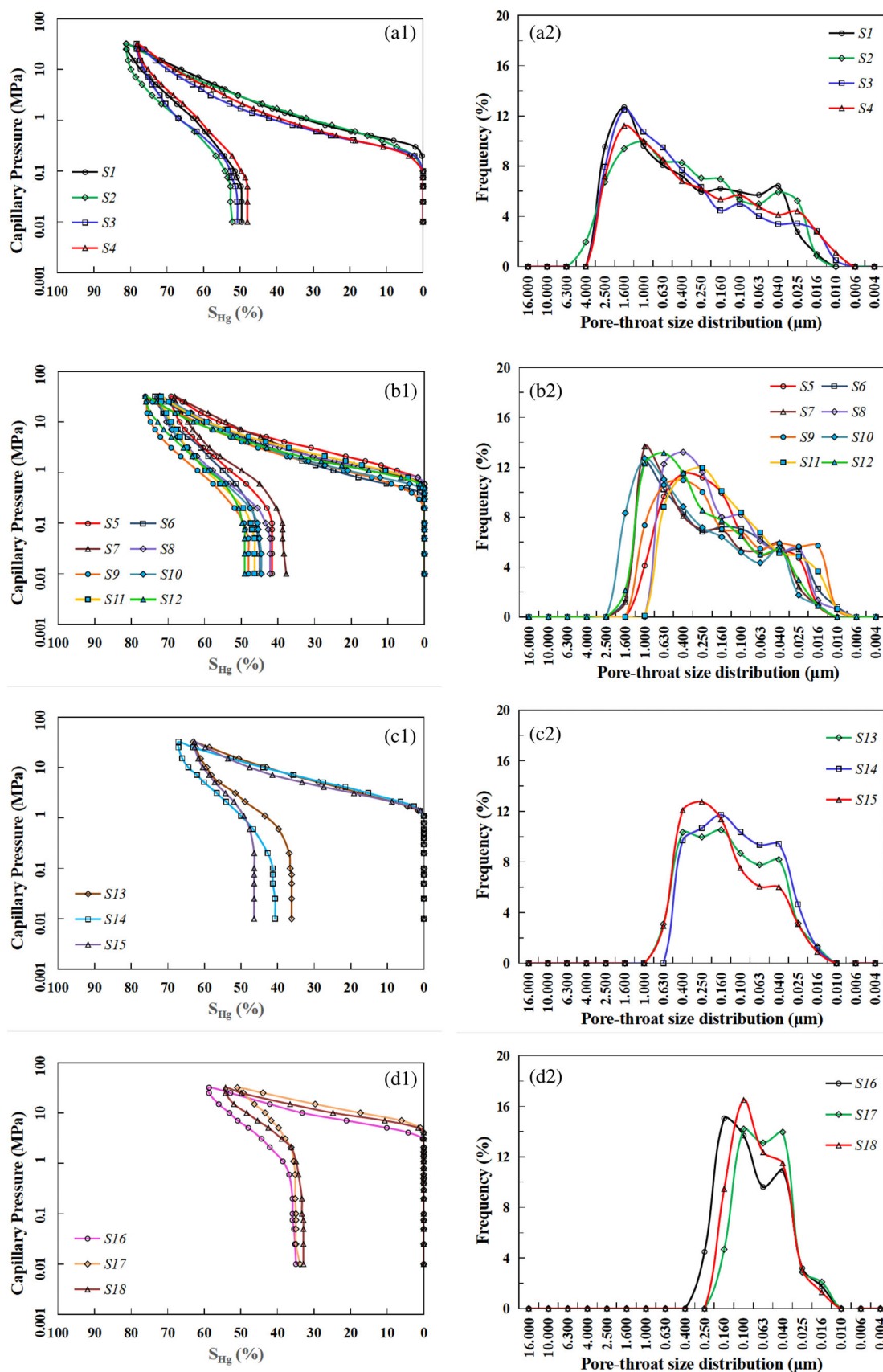


FIGURE 8 Mercury injection and withdrawal curves (a₁, b₁, c₁, d₁) and distributions of pore throat size (a₂, b₂, c₂, d₂) produced from HPMI. Type I-IV (a-d).

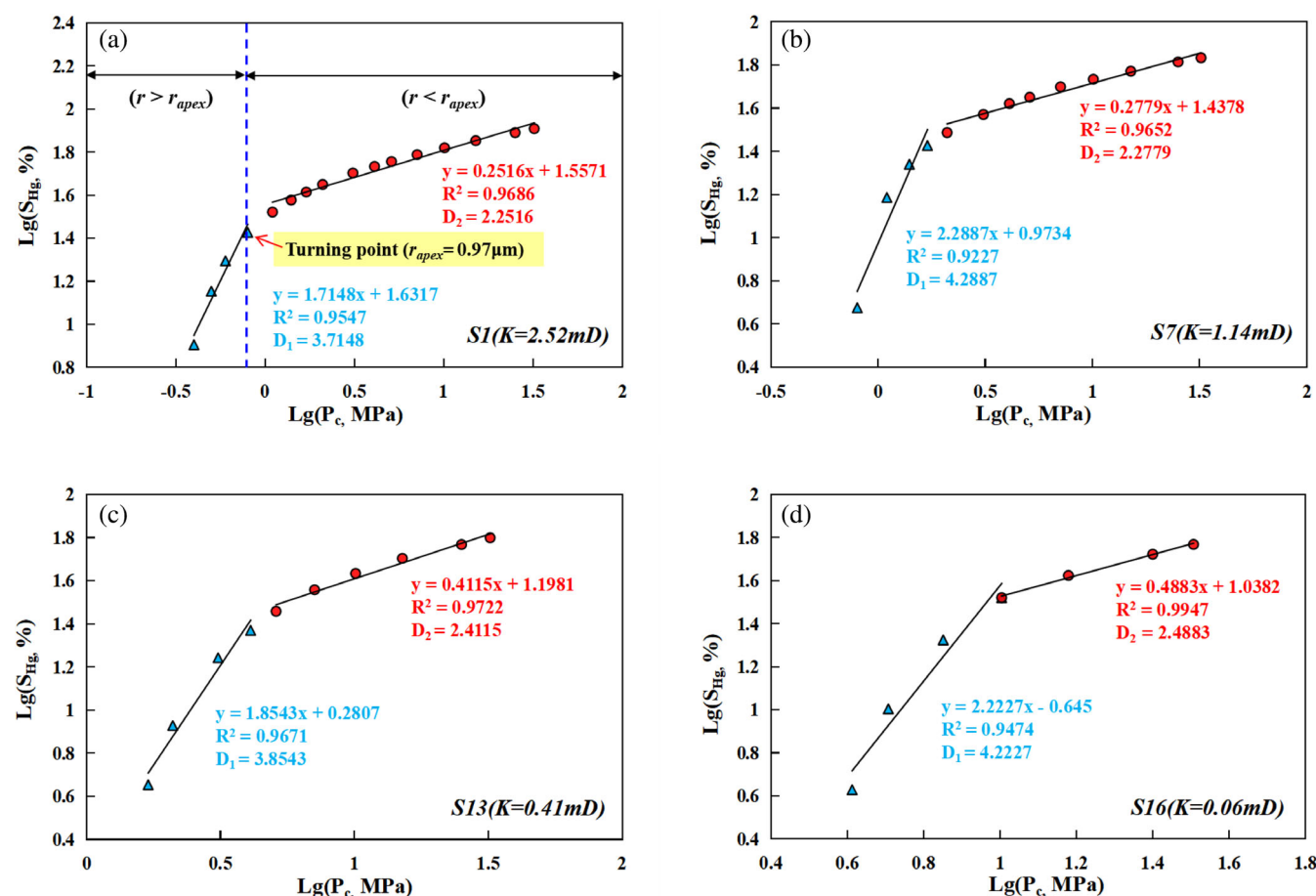


FIGURE 9 $\text{Lg}(S_{Hg}) - \text{Lg}(P_c)$ intersection diagram and fractal dimension calculation of four typical sandstone samples.

for more than 8%, indicating that the large throat has certain advantages and good connectivity (Figure 8a₂).

The mercury injection curve position of type II samples is slightly higher than type I (Figure 8b₁). The threshold pressure is relatively high, ranging from 0.43 to 0.95 MPa, with a mean of 0.66 MPa. However, the median pressure was between 4.13 and 7.09 MPa, averaging 5.6 MPa. The maximum pore throat radius is between 0.79 and 1.76 μm , averaging 1.22 μm , while the average pore throat radius is between 0.19 and 0.4 μm , averaging 0.14 μm . The sorting coefficient is 0.22. The porosity and permeability range from 8.8% ~ 10.9% and 0.67 ~ 1.14 mD, respectively. The type II sample pore throat size shows a single peak, and the range is between 0.016 and 1.6 μm , with a higher distribution frequency of 0.1 ~ 1.0 μm (Figure 8b₂). It is the predominant sandstone type in the research area.

The maximum mercury saturation of type III samples is significantly lower than that of types I and II. The mercury injection curve platform is narrowed (Figure 8c₁), and the threshold samples' pressure is further increased, with a mean of 1.69 MPa. The median pressure is generally greater than 10 MPa, averaging 13.27 MPa. The maximum pore throat radius is less than 0.5 μm , averaging 0.45 μm . However, the average pore throat radius is about 0.1 μm , and the median radius is 0.057 μm on average. The sorting coefficient is small, with a mean of 0.077. However, the skewness

coefficient is large, with an average of 2.29, which reflects good sorting and coarse skewness, while worse permeability (<0.5 mD). The pore throat size of the type III sample exhibits a small-amplitude bimodal distribution with a significantly tight distribution, spanning from 0.016 to 0.63 μm (Figure 8c₂).

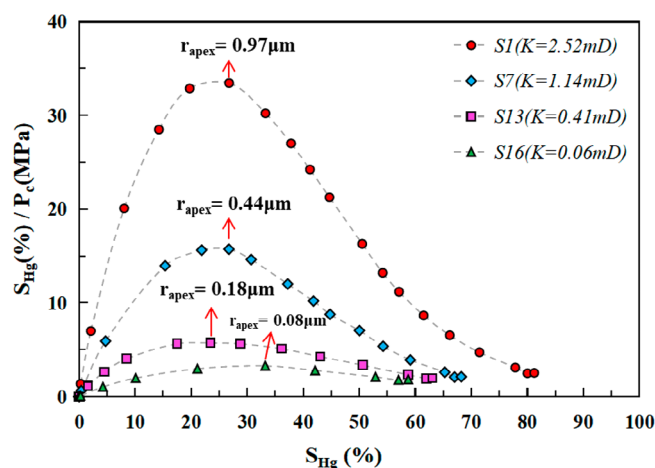
Type IV samples have the smallest maximum mercury saturation (Figure 8d₁; generally <60%). The threshold pressure of the sample is the largest, with a mean of 5.05 MPa. However, the pore throat radius is less than 0.2 μm (averaging 0.17 μm), while the average pore throat radius and median radius are 0.05 and 0.027 μm . The sorting coefficient is the smallest, with a mean of 0.023. The skewness coefficient is large, averaging 2.30. The physical properties of sandstone have significantly deteriorated, and the permeability is less than 0.1 mD. The type IV sample pore throat size presents a restricted and high bimodal distribution, with a distribution range of 0.04 ~ 0.16 μm , showing the characteristics of tight sandstone reservoirs (Figure 8d₂).

4.4 | Pore-throat fractal characteristics based on HPMT data

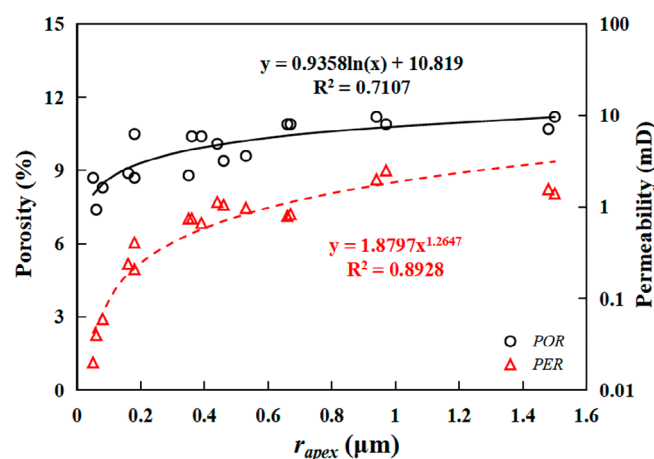
The $\text{Lg}(S_{Hg}) - \text{Lg}(P_c)$ intersection diagram of Chang 6 sandstone samples of the Xiaojiahe area shows that all samples can be divided into

TABLE 2 Fractal dimension calculation results of the Chang 6 sandstone samples in the Xiaojiahe area.

Type	Samples	S_{Hg}/P_c (%/MPa)	r_{apex} (μm)	$r > r_{apex}$		$r < r_{apex}$		D_{ave}	D_p
				D_1	R^2	D_2	R^2		
I	S1	33.54	0.97	3.72	0.955	2.25	0.969	2.63	2.27
	S2	31.18	0.94	3.26	0.991	2.27	0.951	2.51	2.28
	S3	50.41	1.48	3.44	0.965	2.19	0.922	2.53	2.21
	S4	47.41	1.5	3.35	0.970	2.24	0.923	2.52	2.25
II	S5	10.25	0.36	3.62	0.994	2.32	0.922	2.61	2.36
	S6	22.6	0.67	3.99	0.915	2.28	0.966	2.78	2.32
	S7	15.73	0.44	4.29	0.923	2.28	0.965	2.98	2.34
	S8	14.48	0.39	3.50	0.965	2.25	0.966	2.64	2.29
	S9	20.24	0.66	3.42	0.987	2.30	0.927	2.64	2.34
	S10	19.42	0.53	4.19	0.933	2.26	0.940	2.91	2.31
	S11	13.01	0.35	3.86	0.961	2.27	0.943	2.81	2.34
	S12	16.71	0.46	3.97	0.968	2.28	0.931	2.80	2.32
III	S13	5.72	0.18	3.85	0.967	2.41	0.972	2.88	2.53
	S14	5.41	0.16	3.63	0.972	2.41	0.983	2.84	2.54
	S15	6.68	0.18	4.16	0.959	2.33	0.950	3.06	2.47
IV	S16	3.29	0.08	4.22	0.947	2.49	0.995	3.41	2.86
	S17	1.97	0.05	4.08	0.952	2.73	0.997	3.44	3.16
	S18	2.46	0.06	4.40	0.999	2.68	0.973	3.24	2.88

**FIGURE 10** The intersection diagram of S_{Hg}/P_c value and mercury saturation of sandstone samples.

two sections for fractal analysis (Figure 9). The former represents a relatively large pore throat, and the latter depicts a relatively small pore throat. The two sections have good regression fitting ($R^2 > 0.9$; Figure 9a; Table 2). The statistical analysis presents the pore throat radius of the fractal turning point as associated with the pore throat radius r_{apex} at the apex of the Pittman curve (Lai & Wang, 2015). Typically, a maximum apex of S_{Hg}/P_c can be easily found by the $(S_{Hg}/P_c) - (S_{Hg})$ cross plot (Swanson, 1981), and the matching pore throat radius is known as the r_{apex} (Nabawy et al., 2009; Pittman, 1992). Figure 10 presents the intersection diagram of

**FIGURE 11** Relationship between r_{apex} value and porosity and permeability.

S_{Hg}/P_c value and mercury saturation for four types of typical sandstone samples, and the corresponding r_{apex} ranges from 0.05 to 1.5 μm (Table 2). The average value of r_{apex} gradually declines from type I (1.22 μm), type II (0.48 μm), type III (0.173 μm) and type IV sandstone (0.063 μm). However, the corresponding $S_{Hg}(\%)/P_c(\text{MPa})$ value of r_{apex} ranges from 1.97 to 50.41, which gradually decreases from type I to type IV sandstone (Figure 10). There is a strong positive connection between r_{apex} with porosity and permeability (Figure 11: R^2 0.7107 and 0.8928) indicating that this fractal model can accurately describe the reservoir heterogeneity.

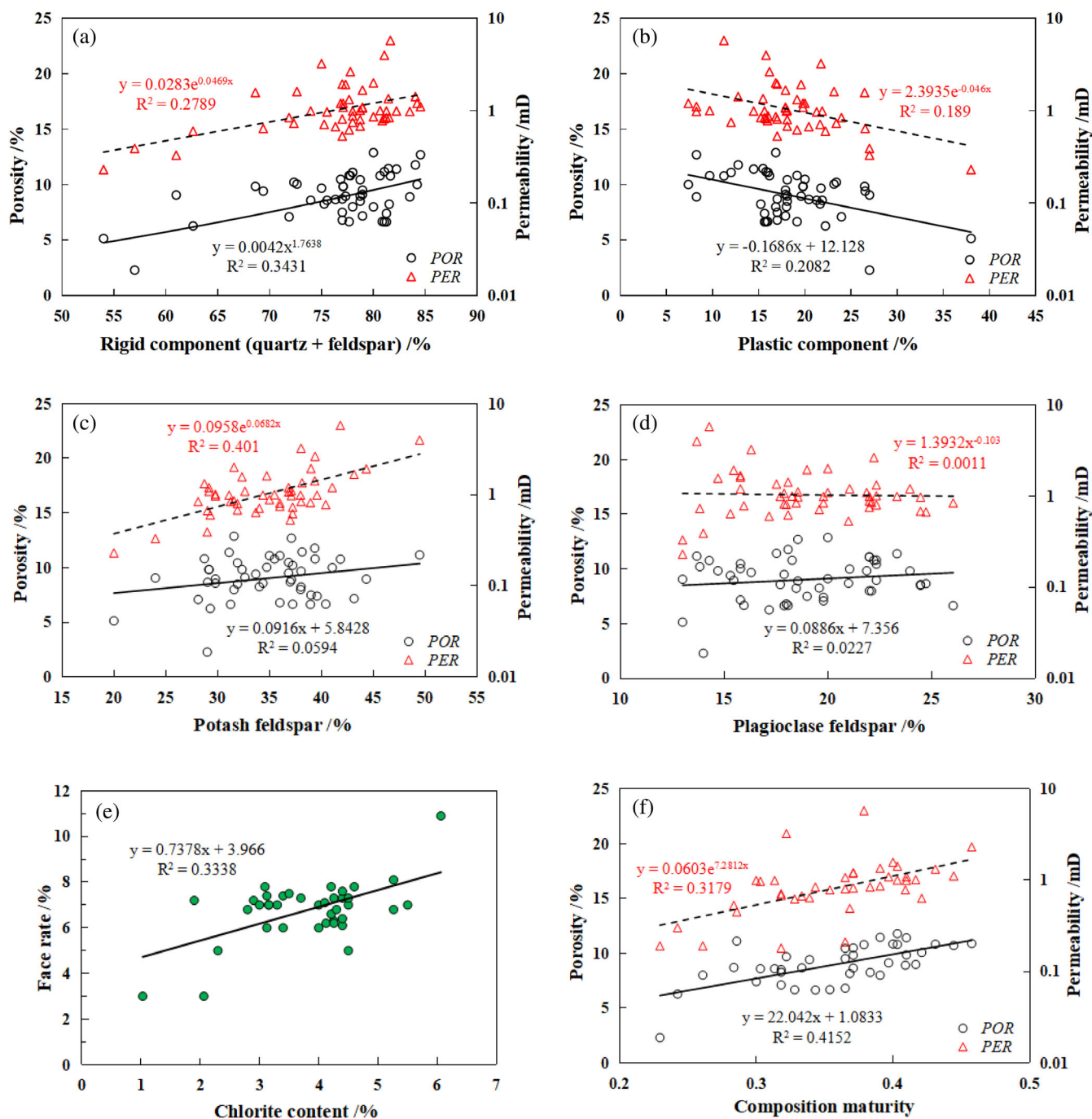


FIGURE 12 Correlation analysis of clastic components with porosity and permeability of Chang 6 sandstone in the Xiaojiahe area.

The fractal dimension obtained by greater than the r_{apex} value is recorded as D_1 , and the fractal dimension obtained by a smaller r_{apex} value is recorded as D_2 . The comprehensive fractal dimension can better characterize the uniformity of pores (Feng et al., 2021; Su et al., 2018). According to the pore throat volume (ϕ_1 , ϕ_2) and capillary pressure difference (ΔP_1 , ΔP_2) corresponding to the intervals of D_1 and D_2 , perform the weighted average calculation to obtain the comprehensive fractal dimensions D_{ave} (Equation 10) and D_p (Equation 11). The fractal dimension calculation results in

Table 2 show that the D_1 ranged from 3.26 to 4.40, averaging 3.83. The D_2 is between 2.19 and 2.73, with an average of 2.35. The D_{ave} ranges from 2.51 to 3.44, with a mean of 2.85, and the D_p varies between 2.21 and 3.16, averaging 2.45.

$$D_{\text{ave}} = \frac{D_1 \times \phi_1 + D_2 \times \phi_2}{\phi_1 + \phi_2} \quad (10)$$

$$D_p = \frac{D_1 \times \Delta P_1 + D_2 \times \Delta P_2}{\Delta P_1 + \Delta P_2} \quad (11)$$

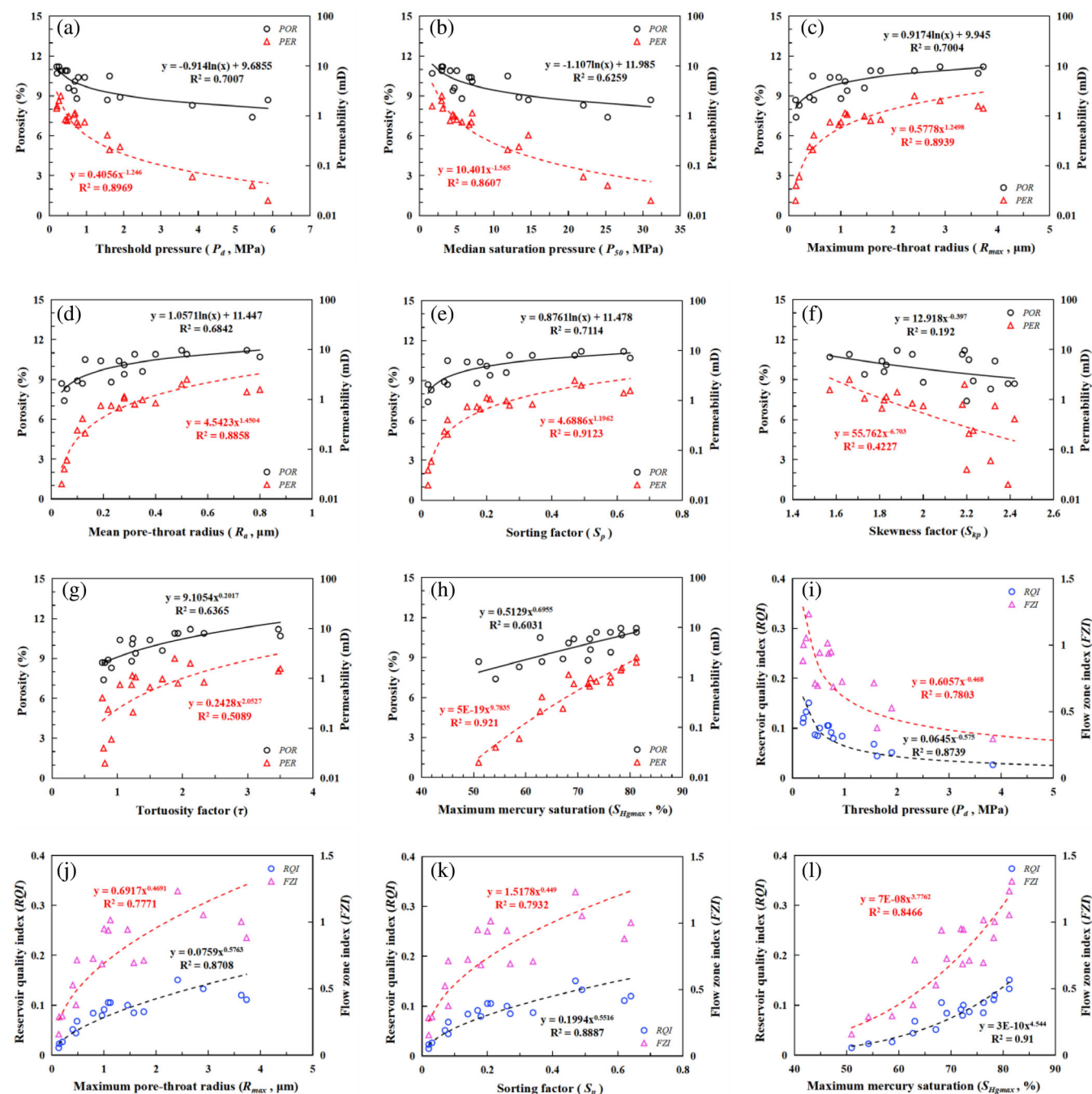


FIGURE 13 The relationships between the physical properties and pore-throat structure parameters obtained from HPMI.

5 | DISCUSSION

5.1 | Effect of detrital components on reservoir physical properties

Detrital components include rigid components such as quartz and feldspar and plastic components, such as biotite, lithic fragment, and cement. These components were the material basis for diagenetic transformation, and their content greatly influences the compression resistance of framework grains and the preservation of

primary pores (Zhao et al., 2016). The correlation between the detrital composition content and physical properties deciphers the rigid components (quartz and feldspar) and positively correlates with porosity and permeability (Figure 12a). In contrast, the content of plastic components, such as biotite and interstitial material negatively correlates with physical properties (Figure 12b), which reflects the plastic components are easily compacted and deformed to form pseudo-hetero groups, and the intergranular pores are further filled. The average amount of potassium feldspar is 34.85%, significantly positively associated with permeability, but

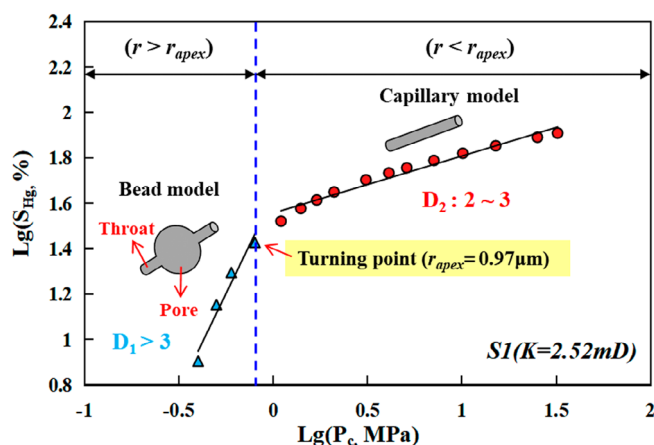


FIGURE 14 Binary pore-throat structure model of ultra-low permeability sandstone (after Zhu et al., 2019).

its effect on porosity is relatively weak (Figure 12c). It indicates the higher concentration of potassium feldspar in the sandstone is beneficial for improving permeability. However, plagioclase is in a small proportion (averaging 18.97%) and has a weak impact on porosity and permeability (Figure 12d). The chlorite cement of the Chang 6 reservoir is in the early or middle stage. With a film-like shape and is prone to form a ring edge (Figure 7b), making it difficult to slide between sandstone framework grains and more stable and decreasing the damage of compaction on reservoir space (Dou et al., 2018). There is a positive correlation between chlorite content and face rate (Figure 12e), confirming the protective effect of thin-film chlorite cement on intergranular pores. The component maturity ($Q/(F + R)$) of sandstone has a good positive relationship with porosity and permeability (Figure 12f), indicating that the more rigid the component content, the better the preservation of primary pores. In addition, the impact of various physical parameters, such as grain size, sorting, and roundness of detrital materials that characterize the structural characteristics of sandstone in the reservoir cannot be ignored.

5.2 | Relationship between pore-throat structure parameters and reservoir physical properties

The control of pore throat size and connectivity on the physical properties cannot be ignored, especially the influence on permeability (Lai, Wang, Cao, et al., 2018; Lai, Wang, Wang, et al., 2018; Wang, Chi, et al., 2018; Wang, Jiao, et al., 2018). The correlation analysis between pore throat structure parameters and physical properties (Figure 13) shows that the threshold pressure (P_d) and the median pressure (P_{50}) are negatively correlated with physical properties. Still, the effects on porosity and permeability are different, with a permeability R^2 of 0.8969, 0.8607, and porosity R^2 of 0.7007, 0.6259, respectively. The maximum pore throat radius (R_{max}), the average pore throat radius (R_a), the sorting factor (S_p), and the maximum mercury saturation (S_{Hgmax}) are positively correlated with the physical properties, and the

R^2 with permeability is 0.8939, 0.8858, 0.9123, 0.921, and with porosity 0.7004, 0.6842, 0.7114, and 0.6031, respectively. It indicates that these pore throat parameters have a significant effect on permeability and a weak effect on porosity. The mercury injection tortuosity (τ) has a positive correlation with physical properties, but the R^2 is lower than the first six parameters. The R^2 for porosity is 0.6365, slightly higher than the permeability R^2 (0.5089). The skewness coefficient (S_{kp}) has a weak negative correlation with physical properties. Similarly, the P_d , R_{max} , S_p , S_{Hgmax} , and other parameters have a good correlation with RQI and FZI values ($R^2 > 0.78$), indicating that these pore throat structure parameters are closely related to reservoir quality evaluation. Therefore, there are more representative parameters such as the lower the P_d and P_{50} values, the higher the R_{max} and R_a values, and the better the reservoir's physical properties, especially the impact on permeability.

5.3 | Effect of fractal characteristics on reservoir physical properties

Fractal dimension can quantitatively characterize the reservoir's heterogeneity, and as the fractal dimension increases, the pore structure gets more intricate (Lai, Wang, Cao, et al., 2018; Lai, Wang, Wang, et al., 2018; Li, 2010). Theoretically, the fractal dimension of three-dimensional varies between 2 and 3. However, many scholars have discussed the reason why the D_1 of the relatively large pore throat part is greater than 3 (Lai & Wang, 2015; Zhu et al., 2019). One explanation was that the simple shape of large pores or the relatively developed micro-fractures led to the oversimplification of the columnar core in the mercury injection process (Lai & Wang, 2015). In addition, previous studies suggested that the pore throat structure of sandstone has a binary structure (Zhu et al., 2019). When the pore throat radius exceeds the turning point radius (r_{apex}), the pore structure is approximate to the bead model (Figure 14), the pore radius is remarkably greater than the throat radius, and the fractal dimension is greater than three, without fractal characteristics. When the pore throat radius is smaller than the r_{apex} , the pore structure is close to the capillary model (Figure 14), the pore radius is similar to the throat radius, and the span of fractal dimension is 2 ~ 3, with fractal characteristics.

The fractal dimension D_1 has a poor correlation with the porosity, permeability, RQI, and FZI (Figure 15a,b), the correlation coefficient R^2 with the physical properties of the reservoir is less than 0.5, while the correlation coefficient R^2 with the RQI and FZI parameters is less than 0.3, indicating D_1 cannot characterize the heterogeneity of the reservoir. The correlation between fractal dimension D_2 and the above four parameters (Figure 15c,d) shows that except for the correlation coefficient R^2 with porosity ($R^2 = 0.6018$), the other three parameters have a higher R^2 (> 0.8). The comprehensive fractal dimensions D_{ave} and D_p have a good correlation with reservoir physical properties and reservoir quality parameters (except with porosity $R^2 < 0.6$) (Figure 15e-h), and D_p has a more significant effect on permeability and RQI, with a corresponding R^2 of 0.9401 and 0.9317.

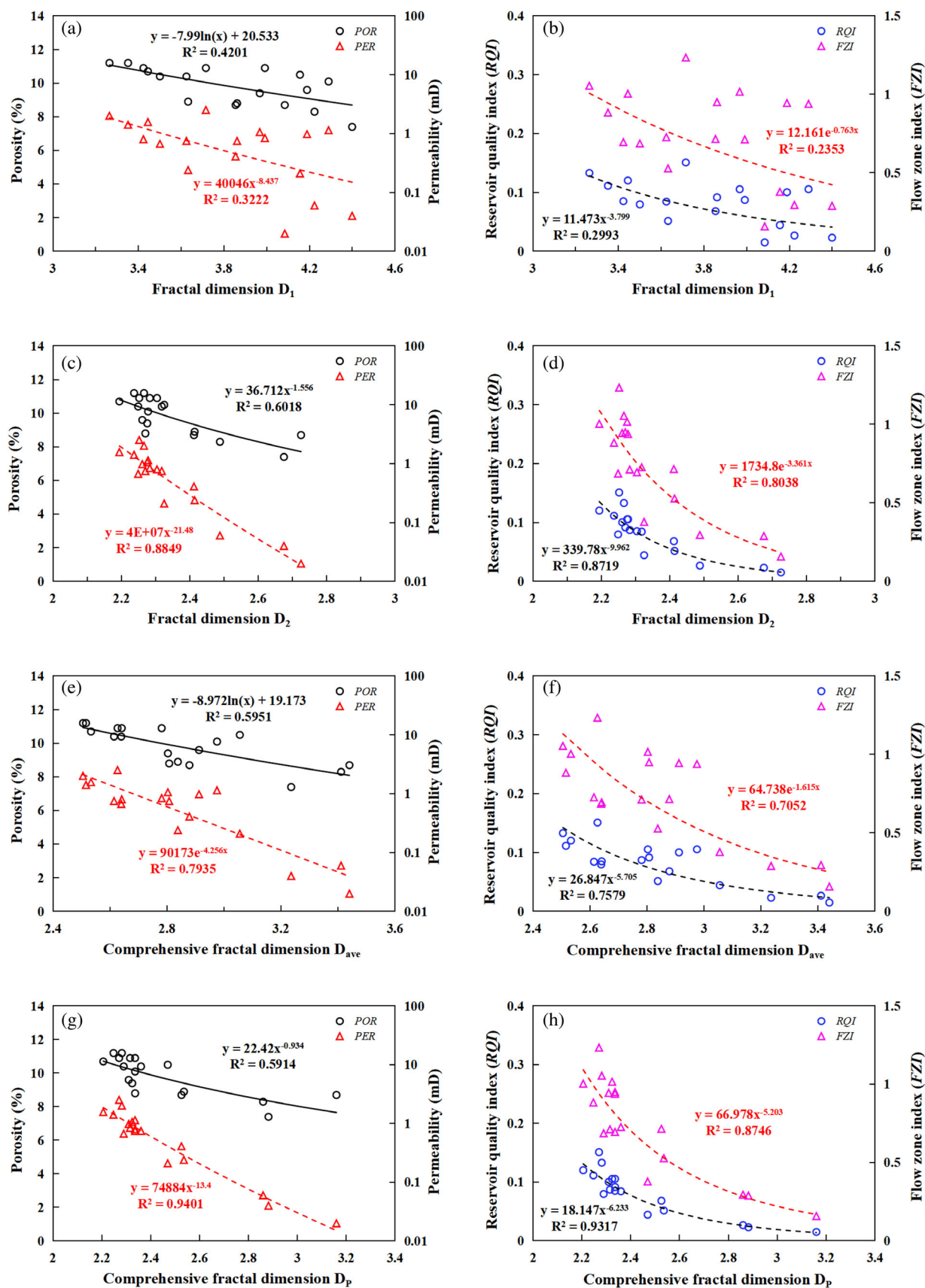


FIGURE 15 Relationship between different fractal dimensions (D_1 , D_2 , D_{ave} , and D_p) and reservoir physical properties and reservoir quality parameters.

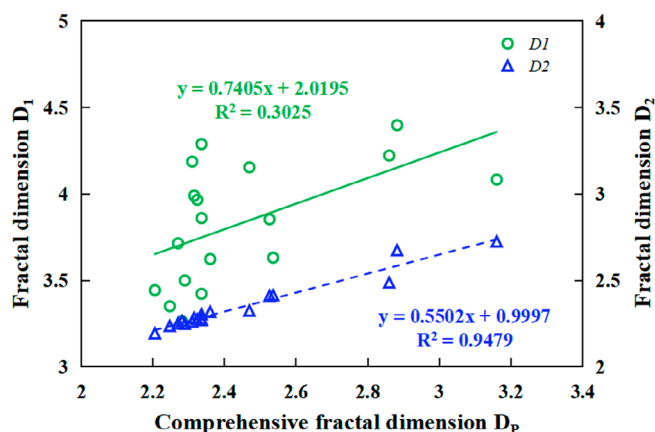


FIGURE 16 Relationship between comprehensive fractal dimension D_p and D_1 , D_2

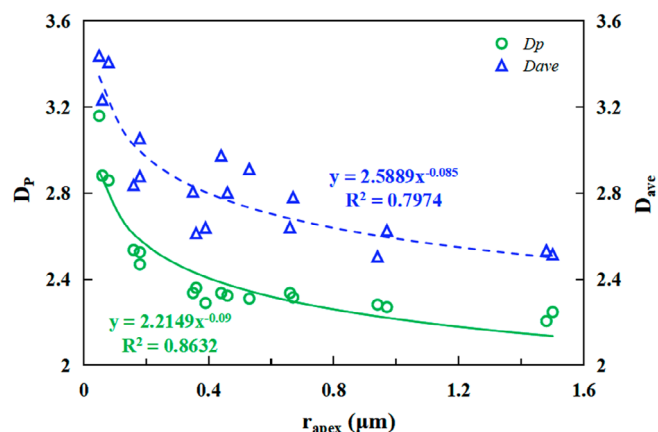


FIGURE 17 Relationship between r_{apex} and comprehensive fractal dimension D_p , D_{ave}

TABLE 3 The maximum contribution radius, hyperbolic apex radius, and other scale pore-throat parameters of the Chang 6 sandstone in the Xiaojiage area.

Type	Samples	Parameters related to R_{mp} and r_{apex}						Non-nano and nanoscale pore throat					
		R_{mp} (μm)	S_{Hg-mp} (%)	CP_{mp} (%)	r_{apex} (μm)	$S_{Hg-apex}$ (%)	CP_{apex} (%)	S_{Hg} $r > 0.1$	$CP_{r > 0.1}$	$Por_{r > 0.1}$ (%)	$Por_{r < 0.1}$ (%)	Por_{em} (%)	Por_{fem} (%)
I	S1	1.65	13.93	56.15	0.97	25.96	87.85	61.47	99.91	6.70	2.15	3.44	2.05
	S2	1.68	14.58	65.29	0.94	24.95	87.52	63.45	99.93	7.11	1.99	3.25	2.11
	S3	2.53	11.53	51.22	1.48	25.32	87.31	66.58	99.98	7.12	1.26	2.96	2.31
	S4	2.52	10.87	50.37	1.5	23.71	87.02	64.29	99.97	7.20	1.56	3.38	2.44
II	S5	0.63	10.12	37.89	0.36	21.52	80.24	50.39	99.11	5.24	1.96	2.87	3.20
	S6	1.02	16.1	72.62	0.67	24.86	87.15	55.19	99.84	6.02	2.00	3.11	2.89
	S7	0.68	15.35	72.25	0.44	26.74	87.82	50.03	99.63	5.05	1.83	3.08	3.21
	S8	0.62	15.12	60.77	0.39	26.92	86.82	54.09	99.57	5.63	1.89	3.13	2.89
	S9	1.04	13.52	52.05	0.66	22.25	80.04	58.02	99.76	6.32	1.98	3.07	2.59
	S10	1.01	10.46	52.52	0.53	27.18	88.01	55.73	99.81	5.35	1.60	2.67	2.65
	S11	0.65	11.63	55.06	0.35	27.57	87.34	53.73	99.42	4.73	1.60	2.25	2.47
	S12	0.62	16.21	69.19	0.46	27.62	86.56	57.72	99.63	5.43	1.74	2.56	2.23
III	S13	0.26	16.35	73.67	0.18	24.11	86.78	36.18	96.63	3.15	2.34	2.34	3.21
	S14	0.25	15.25	57.83	0.16	25.16	83.92	35.67	94.15	3.17	2.80	2.35	2.93
	S15	0.27	17.62	72.02	0.18	27.00	87.25	41.42	97.45	4.35	2.24	1.71	3.91
IV	S16	0.11	18.64	77.48	0.08	32.22	87.86	21.13	77.48	1.75	3.12	1.97	3.43
	S17	0.065	20.45	77.51	0.05	29.69	87.92	6.08	35.38	0.53	3.90	1.49	4.27
	S18	0.13	12.21	50.83	0.06	31.64	87.58	10.65	50.83	0.79	3.22	1.58	3.39

Abbreviations: CP_{apex} , cumulative permeability contribution value corresponding to r_{apex} ; CP_{mp} , cumulative permeability contribution value corresponding to R_{mp} ; $CP_{r > 0.1}$, cumulative permeability contribution value corresponding to the non-nanoscale pore throat ($r > 0.1 \mu m$); Por_{em} , the effective movable pore throat volume; Por_{fem} , the pore throat volume of failure to enter mercury; $Por_{r < 0.1}$, the nanoscale pore throat volume ($r < 0.1 \mu m$); $Por_{r > 0.1}$, the non-nanoscale pore throat volume ($r > 0.1 \mu m$); r_{apex} , Pittman's plot apex radius; R_{mp} , pore throat radius of the maximum permeability contribution value; $S_{Hgr > 0.1}$, mercury injection saturation corresponding to the non-nanoscale pore throat ($r > 0.1 \mu m$); $S_{Hg-apex}$, mercury injection saturation corresponding to r_{apex} ; S_{Hg-mp} , mercury injection saturation corresponding to R_{mp} .

The physical properties and quality of the reservoir deteriorated with the increased fractal dimension. The correlation between D_p and D_1 was poor ($R^2 = 0.3025$). However, it has a strong linear positive correlation with D_2 ($R^2 = 0.9479$; Figure 16). Moreover, D_p gradually

declines with the increase in r_{apex} , showing a strong negative correlation ($R^2 = 0.8632$; Figure 17). Therefore, the D_2 of relatively small pores ($r < r_{apex}$) and the D_p are preferable to depict the complexity and heterogeneity of the pore throat structure in ultra-low permeability

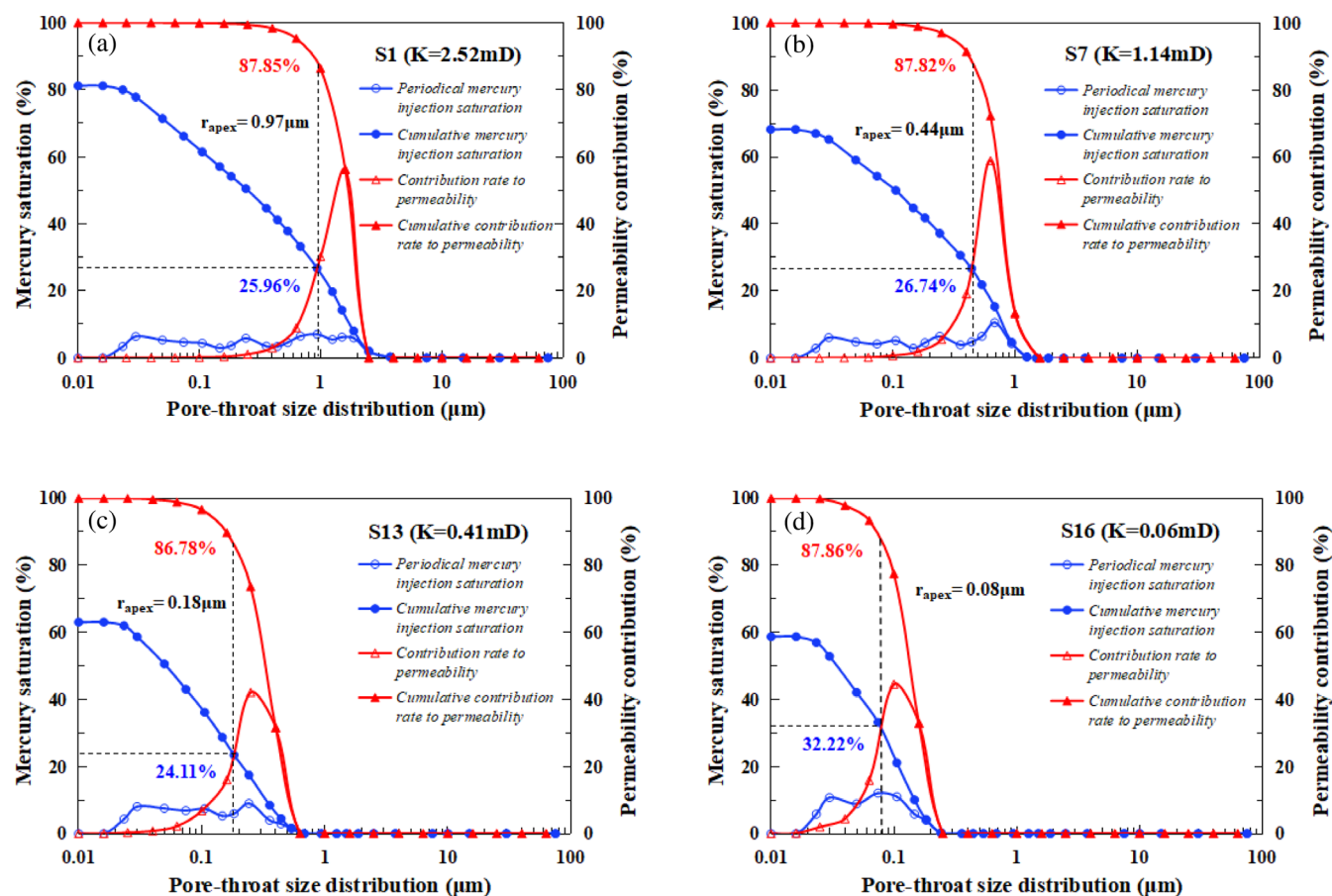


FIGURE 18 The distribution relationship between pore throat size and mercury saturation and permeability contribution value for four types of typical sandstone samples (S1, S7, S13, and S16) from type I to type IV.

sandstone. From type I to type IV sandstone, the larger D_2 , and D_p , the stronger heterogeneity.

5.4 | Controlling of the pore-throat size scale on reservoir physical properties

5.4.1 | Effect of pore-throat associated with R_{mp} and r_{apex} on physical properties

Previous studies suggest the larger pore throats constitute the pore geometry, but narrow throats are critical for connectivity (Lai, Wang, Wang, et al., 2018; Schmitt et al., 2015). Pore throat size and distribution characteristics have a more significant effect on permeability than total porosity (Lai, Wang, Cao, et al., 2018; Rezaee et al., 2012). The r_{apex} obtained by the Pittman plot represents a transition from a narrow pore throat with poor connectivity to a wide pore throat with good connectivity (Lai & Wang, 2015; Nabawy et al., 2009; Pittman, 1992; Swanson, 1981). This research has calculated the mercury injection saturation and permeability contribution value matching to the r_{apex} and the pore throat radius of the maximum permeability contribution value (R_{mp}) in the Chang 6 ultra-low permeability sandstone (Table 3). The results show the R_{mp} value ($0.065 \mu m \sim 2.53 \mu m$)

of each sandstone sample is slightly larger than the r_{apex} ($0.05 \sim 1.5 \mu m$). The mercury saturation S_{Hg-mp} ($10.12\% \sim 20.45\%$) and cumulative permeability contribution CP_{mp} ($37.89\% \sim 77.51\%$) relative to R_{mp} are smaller than the mercury saturation $S_{Hg-apex}$ ($21.52\% \sim 32.22\%$) and cumulative permeability contribution CP_{apex} ($80.04\% \sim 88.01\%$) corresponding to the r_{apex} value. Therefore, the r_{apex} value can better characterize the change in pore throat connectivity.

Figure 18 presents the relationship of pore throat radius with mercury saturation and permeability contribution in the studied four typical sandstones. It deciphers the permeability decreases from type I to type IV sandstone. According to the r_{apex} value, the corresponding parameters in the pore throat size range of $r > r_{apex}$ and $r < r_{apex}$ can be divided into two parts for discussion. The cumulative mercury saturation slowly increases when the pore throat radius is greater than the r_{apex} ($r > r_{apex}$), but the cumulative permeability contribution rapidly increases ($>80\%$). The corresponding mercury injection saturation at the r_{apex} value of four samples (S1, S7, S13, and S16) is 25.96%, 26.74%, 24.11%, and 32.22%, while the cumulative permeability contribution values are 87.85%, 87.82%, 86.78%, and 87.86%, respectively (Figure 18). It indicates that the small proportion of large pores significantly contributed to permeability (Figure 18). When the pore throat radius is smaller than the r_{apex} ($r < r_{apex}$), the cumulative

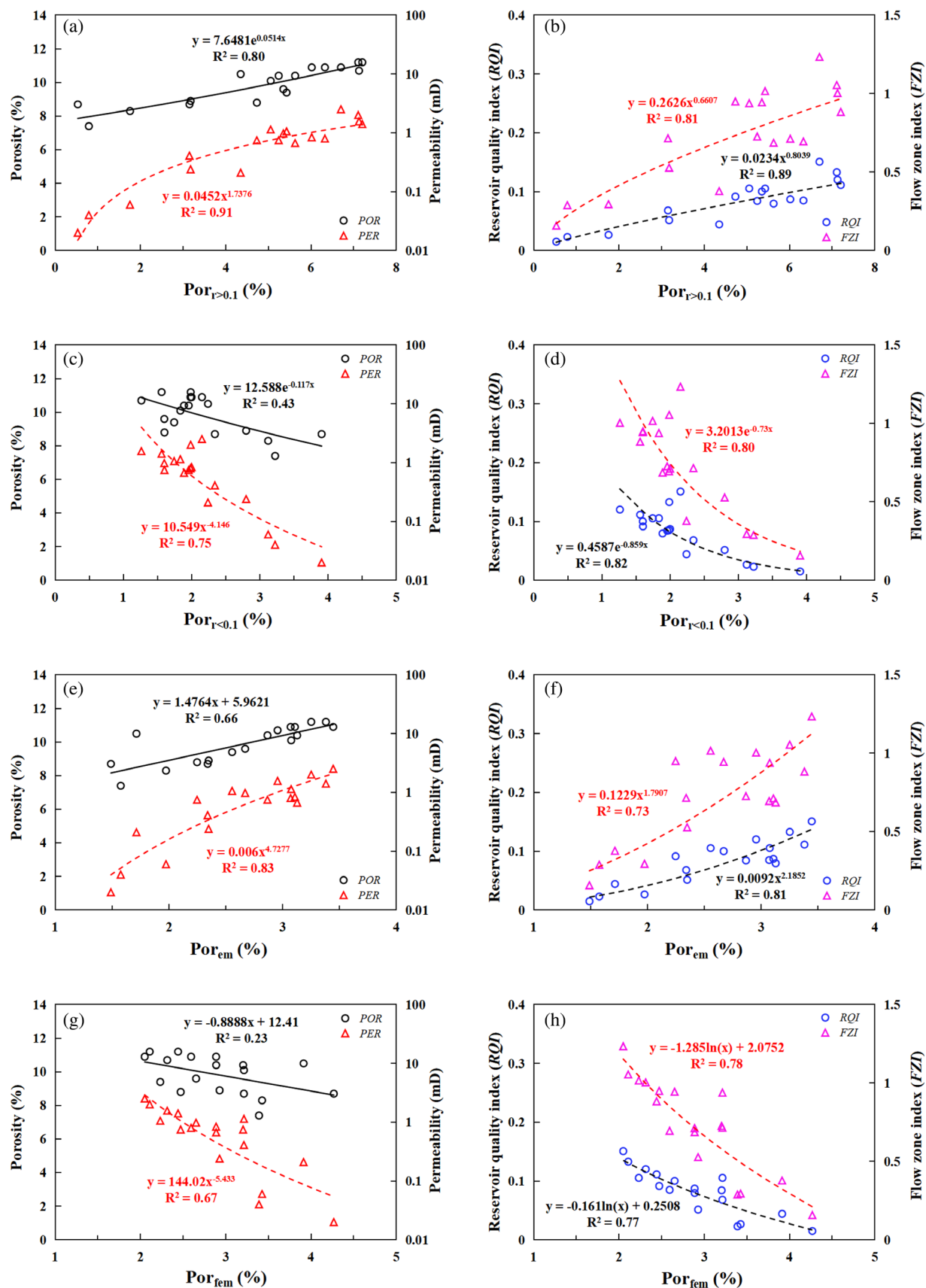


FIGURE 19 The correlation relationship between $\text{Por}_{r>0.1}$, $\text{Por}_{r<0.1}$, Por_{em} , Por_{fem} , and reservoir physical properties, reservoir quality parameters.

mercury saturation continues to increase, but the cumulative permeability contribution rises slowly. The relatively narrow pore throat interval occupied more mercury injection saturation and largely contributed to the total porosity and less impacted permeability contribution.

5.4.2 | Influence of other scale pore-throat on physical properties

The relationship between total porosity and permeability is relatively poor (Figure 5; $R^2 = 0.469$) due to the intricate pore throat structure and strong heterogeneity of ultra-low permeability sandstone. However, the influence of different grades of pore throats on permeability has a discrepancy (Lai, Wang, Cao, et al., 2018; Rezaee et al., 2012). The pore throat radius $r < 0.1 \mu\text{m}$ is called nanoscale pore throat, while the pore throat radius $r > 0.1 \mu\text{m}$ is non-nanoscale pore throat. The nanoscale pore throat volume ($\text{Por}_{r<0.1}$) and the non-nanoscale pore throat volume ($\text{Por}_{r>0.1}$) are obtained by the corresponding mercury saturation at $r = 0.1 \mu\text{m}$ (Table 3). In addition, the effective movable pore throat volume (Por_{em}) and the pore throat volume of failure to enter mercury (Por_{fem}) can be obtained by S_{Hgmax} and W_E (Table 3).

The results in Table 3 show the mercury saturation ($S_{\text{Hgr}>0.1}$) in the non-nanoscale pore throat interval with $r > 0.1 \mu\text{m}$ varies from 6.08% to 66.58%. The cumulative permeability contribution value of non-nanoscale pore throats ($\text{CP}_{r>0.1}$) in type I, II, and III sandstone reaches 94.15% ~ 99.98%, and the contribution of nanoscale pore throats ($r < 0.1 \mu\text{m}$) to the permeability of these three sandstones is almost negligible. However, in the type IV sandstone, the permeability decreases ($K < 0.1 \text{ mD}$) and the reservoir becomes tighter, and the cumulative permeability contribution value corresponding to the non-nanoscale pore throat ($r > 0.1 \mu\text{m}$) gradually declines (35.38% ~ 77.48%). Indicating the non-nanoscale pore throat contributes significantly to the permeability of sandstone, and the higher the proportion, the more favourable the physical properties of the reservoir.

Comparing the effects of different types of pore throats ($\text{Por}_{r>0.1}$, $\text{Por}_{r<0.1}$, Por_{em} , Por_{fem}) on physical properties and reservoir quality parameters (Figure 19). The results show that $\text{Por}_{r>0.1}$ and Por_{em} have a strong positive correlation with permeability, R^2 is 0.91 and 0.83, respectively, but the correlation with porosity is relatively low (Figure 19a,e). Furthermore, it has a similar positive trend with RQI and FZI ($R^2 > 0.73$; Figure 19b,f). $\text{Por}_{r<0.1}$ and Por_{fem} have a negative correlation with permeability ($R^2 = 0.75$ and 0.67), RQI ($R^2 = 0.82$ and 0.77), and FZI ($R^2 = 0.80$ and 0.78), but are very poorly correlated with porosity, R^2 is 0.43 and 0.23, respectively (Figure 19c,d,g,h). Indicating that non-nanoscale pore throats and effective movable pore throats have a remarkable contribution to the infiltration capacity of ultra-low permeability sandstone, which is the dominant factor of reservoir quality. The development of nanoscale pore throats and micropore throats that fail to enter mercury is detrimental to seepage performance and reservoir quality.

6 | CONCLUSIONS

1. The Chang 6 reservoir in the Xiaojiahe area of the Ordos Basin is mainly feldspar sandstone with a mean porosity and permeability of 8.95% and 1.14 mD. The pore types are primarily intergranular pores, followed by dissolution pores. The throat types are mostly curved sheets and necking throats. The Chang 6 sandstone can be categorized into four types by analysing the mercury injection curve; the quality of reservoirs from type I to type IV gradually deteriorated.
2. The high content of quartz and feldspar in the detrital components is conducive to improving the porosity and permeability of the reservoir. However, the content of biotite, interstitial, and other plastic components is negatively correlated with their physical properties. The pore-throat structure parameters such as displacement pressure, median pressure, and pore throat radius can characterize the change in reservoir physical properties, especially the effect on reservoir permeability, which is more significant.
3. The $\text{Lg}(S_{\text{Hg}}) - \text{Lg}(P_c)$ fractal curve can be divided into two segments for analysis at r_{apex} as the turning point demonstrating that ultra-low permeability sandstone has a binary structure, and the r_{apex} can well characterize the connectivity of the pore throat. The pore structure of the relatively large pore throat ($r > r_{\text{apex}}$) is close to the beaded model. The capillary model is quite similar to the pore structure of the relatively small pore throat ($r < r_{\text{apex}}$), with good fractal characteristics. The fractal dimensions D_2 and D_p have an excellent correlation with reservoir quality parameters, which can more accurately describe the complexity and heterogeneity of the pore throat structure of ultra-low permeability sandstone.
4. The relatively large pore throats ($r > r_{\text{apex}}$) have apparent control effects on permeability. The relatively small pore throats ($r < r_{\text{apex}}$) contribute more to the total porosity and have less impact on permeability. In addition, non-nanoscale pore throats ($\text{Por}_{r>0.1}$) and effective movable pore throats (Por_{em}) have significant contributions to the percolation capacity of ultra-low permeability sandstone. The development of nanoscale pore throats ($\text{Por}_{r<0.1}$) and micropore throats of failure to enter mercury (Por_{fem}) have adverse effects on reservoir performance.

AUTHOR CONTRIBUTIONS

Guoxiong Li and Professor Chenglin Liu conceived of the presented idea and prepared an original draft. Associate Professor Ya-nan Zhou and Professor Hanning Wu contributed valuable comments and ideas for improvement to this article. Rizwan Sarwar Awan reviewed and edited the article. Fei Shi conducted an investigation and provided resources. Guoxiong Li, Yunfei Wu, Qibiao Zang, and Yuping Wu carried out the experiments, data processing, and graphics compilation. All authors discussed the results and contributed to the final manuscript.

ACKNOWLEDGEMENTS

This work is financially supported by the National Natural Science Foundation of China (grant no. 41872127) and the National Key R&D

Program of China (grant no. 2021YFA0719000). We thank the Exploration and Development Research Institute of Zichang Oil Production Plant for providing a database.

PEER REVIEW

The peer review history for this article is available at <https://publons.com/publon/10.1002/gj.4700>.

DATA AVAILABILITY STATEMENT

Research data are not shared.

ORCID

Guoxiong Li  <https://orcid.org/0000-0002-7505-1887>

Chenglin Liu  <https://orcid.org/0000-0001-9075-5228>

Rizwan Sarwar Awan  <https://orcid.org/0000-0003-4035-8579>

REFERENCES

- Amaefule, J. O., Altunbay, M., Tiab, D., Kersey, D. G., & Keelan, D. K. (1993). *Enhanced reservoir description: Using core and log data to identify hydraulic (flow) units and predict permeability in uncored intervals/wells: OnePetro*. SPE Annual Technical Conference and Exhibition.
- Angulo, R. F., Alvarado, V., & Gonzalez, H. (1992). *Fractal dimensions from mercury intrusion capillary tests: OnePetro*. SPE Latin America Petroleum Engineering Conference.
- Dou, W., Liu, L., Wu, K., Xu, Z., & Feng, X. (2018). Diagenesis of tight oil sand reservoirs: Upper Triassic tight sandstones of Yanchang Formation in Ordos Basin, China. *Geological Journal*, 53(2), 707–724.
- Dou, W., Liu, L., Xu, Z., Wang, M., Chen, Y., & Wang, X. (2021). Surface fractal analysis of pore structure of tight sandstones: Comparison of different models based on mercury intrusion porosimetry. *AAPG Bulletin*, 105(7), 1491–1509.
- Feng, Z., Zhou, Y., & Wu, W. (2021). Mercury injection fractal characteristics and reservoir evaluation of heterogeneous sandstone reservoirs. *Journal of China University of Petroleum (Edition of Natural Science)*, 6(45), 25–34.
- Folk, R. L., Andrews, P. B., & Lewis, D. W. (1970). Detrital sedimentary rock classification and nomenclature for use in New Zealand. *New Zealand Journal of Geology and Geophysics*, 13(4), 937–968.
- Guo, Y., Liu, J., Yang, H., Liu, Z., Fu, J., Yao, J., ... Zhang, Y. (2012). Hydrocarbon accumulation mechanism of low permeable tight lithologic oil fields in the Yanchang Formation, Ordos Basin, China. *Petroleum Exploration and Development*, 39(4), 447–456.
- Hansen, J. P., & Skjeltorp, A. T. (1988). Fractal pore space and rock permeability implications. *Physical Review B*, 38(4), 2635–2638.
- Hao, L., Tang, J., Wang, Q., Tao, H., Ma, X., Ma, D., & Ji, H. (2017). Fractal characteristics of tight sandstone reservoirs: A case from the Upper Triassic Yanchang Formation, Ordos Basin, China. *Journal of Petroleum Science and Engineering*, 158, 243–252.
- Huang, H., Chen, L., Sun, W., Xiong, F., Ji, W., Jia, J., ... Luo, B. (2018). Pore-throat structure and fractal characteristics of Shihezi Formation tight gas sandstone in the Ordos Basin, China. *Fractals*, 26(2), 1840005.
- Huang, H., Li, R., Xiong, F., Hu, H., Sun, W., Jiang, Z., ... Wu, L. (2020). A method to probe the pore-throat structure of tight reservoirs based on low-field NMR: Insights from a cylindrical pore model. *Marine and Petroleum Geology*, 117, 104344.
- Katz, A. J., & Thompson, A. H. (1985). Fractal sandstone pores: Implications for conductivity and pore formation. *Physical Review Letters*, 54(12), 1325–1328.
- Lai, J., & Wang, G. (2015). Fractal analysis of tight gas sandstones using high-pressure mercury intrusion techniques. *Journal of Natural Gas Science and Engineering*, 24, 185–196.
- Lai, J., Wang, G., Cao, J., Xiao, C., Wang, S., Pang, X., ... Yang, L. (2018). Investigation of pore structure and petrophysical property in tight sandstones. *Marine and Petroleum Geology*, 91, 179–189.
- Lai, J., Wang, G., Wang, Z., Chen, J., Pang, X., Wang, S., ... Fan, X. (2018). A review on pore structure characterization in tight sandstones. *Earth-Science Reviews*, 177, 436–457.
- Li, K. (2010). Analytical derivation of Brooks–Corey type capillary pressure models using fractal geometry and evaluation of rock heterogeneity. *Journal of Petroleum Science and Engineering*, 73(1–2), 20–26.
- Li, W., Pang, J., & Cao, H. (2009). Sedimentary system and lithofacies paleogeographic evolution of the Late Triassic Yanchang period in Ordos Basin. *Journal of Northwest University (Natural Science Edition)*, 39(3), 501–506.
- Liu, C., Yin, C., Lu, J., Sun, L., Wang, Y., Hu, B., & Li, J. (2020). Pore structure and physical properties of sandy conglomerate reservoirs in the Xujiaweizi depression, northern Songliao Basin, China. *Journal of Petroleum Science and Engineering*, 192, 107217.
- Liu, H. Q., Yuan, J. Y., Li, X. B., Wanyan, R., & Liao, J. B. (2007). Lake basin evolution of Ordos Basin during Middle-Late Triassic and its origin analysis. *Lithologic Reservoirs*, 19(1), 52–56.
- Mandelbrot, B. (1982). *The fractal geometry of nature*. WH Freeman. Non-fractality on Large.
- Mandelbrot, B. B. (1975). Stochastic models for the Earth's relief, the shape and the fractal dimension of the coastlines, and the number-area rule for islands. *Proceedings of the National Academy of Sciences United States of America*, 72(10), 3825–3828.
- Nabawy, B. S., Géraud, Y., Rochette, P., & Bur, N. (2009). Pore-throat characterization in highly porous and permeable sandstones. *AAPG Bulletin*, 93(6), 719–739.
- Nelson, P. H. (2009). Pore-throat sizes in sandstones, tight sandstones, and shales. *AAPG Bulletin*, 93(3), 329–340.
- Pittman, E. D. (1992). Relationship of porosity and permeability to various parameters derived from mercury injection-capillary pressure curves for sandstone. *AAPG Bulletin*, 76(2), 191–198.
- Rezaee, R., Saeedi, A., & Clennell, B. (2012). Tight gas sands permeability estimation from mercury injection capillary pressure and nuclear magnetic resonance data. *Journal of Petroleum Science and Engineering*, 88, 92–99.
- Schmitt, M., Fernandes, C. P., Wolf, F. G., Da Cunha Neto, J. A. B., Rahner, C. P., & Dos Santos, V. S. S. (2015). Characterization of Brazilian tight gas sandstones relating permeability and Angstrom-to micron-scale pore structures. *Journal of Natural Gas Science and Engineering*, 27, 785–807.
- Su, P., Xia, Z., Qu, L., Yu, W., Wang, P., Li, D., & Kong, X. (2018). Fractal characteristics of low-permeability gas sandstones based on a new model for mercury intrusion porosimetry. *Journal of Natural Gas Science and Engineering*, 60, 246–255.
- Swanson, B. F. (1981). A simple correlation between permeabilities and mercury capillary pressures. *Journal of Petroleum Technology*, 33(12), 2498–2504.
- Wang, E., Feng, Y., Peng, Y., Li, C., Song, Y., & Liu, G. (2022). Micro- and nanoscale pore-throat structure, fractal characteristics, and permeability estimation models in deep sandstones: Palaeogene Shahejie Formation, Nanpu Sag, NE China. *Geological Journal*, 57(5), 1803–1819.
- Wang, F., Jiao, L., Liu, Z., Tan, X., Wang, C., & Gao, J. (2018). Fractal analysis of pore structures in low permeability sandstones using mercury intrusion porosimetry. *Journal of Porous Media*, 21(11), 1097–1119.
- Wang, F., Yang, K., You, J., & Lei, X. (2019). Analysis of pore size distribution and fractal dimension in tight sandstone with mercury intrusion porosimetry. *Results in Physics*, 13, 102283.
- Wang, J., Wu, S., Li, Q., & Guo, Q. (2020). An investigation into pore structure fractal characteristics in tight oil reservoirs: A case study of the Triassic tight sandstone with ultra-low permeability in the Ordos Basin, China. *Arabian Journal of Geosciences*, 13(18), 1–16.

- Wang, J., Wu, S., Li, Q., Zhang, J., & Guo, Q. (2020). Characterization of the pore-throat size of tight oil reservoirs and its control on reservoir physical properties: A case study of the Triassic tight sandstone of the sediment gravity flow in the Ordos Basin, China. *Journal of Petroleum Science and Engineering*, 186, 106701.
- Wang, R., Chi, Y., Zhang, L., He, R., Tang, Z., & Liu, Z. (2018). Comparative studies of microscopic pore throat characteristics of unconventional super-low permeability sandstone reservoirs: Examples of Chang 6 and Chang 8 reservoirs of Yanchang Formation in Ordos Basin, China. *Journal of Petroleum Science and Engineering*, 160, 72–90.
- Wang, Y., Liu, L., Li, S., Ji, H., Xu, Z., Luo, Z., ... Li, L. (2017). The forming mechanism and process of tight oil sand reservoirs: A case study of Chang 8 oil layers of the Upper Triassic Yanchang Formation in the western Jiyuan area of the Ordos Basin, China. *Journal of Petroleum Science and Engineering*, 158, 29–46.
- Wang, Z., Luo, X., Lei, Y., Zhang, L., Shi, H., Lu, J., ... He, Y. (2020). Impact of detrital composition and diagenesis on the heterogeneity and quality of low-permeability to tight sandstone reservoirs: An example of the Upper Triassic Yanchang Formation in Southeastern Ordos Basin. *Journal of Petroleum Science and Engineering*, 195, 107596.
- Washburn, E. W. (1921). The dynamics of capillary flow. *Physical Review*, 17(3), 273–283.
- Wu, Y., Liu, C., Ouyang, S., Luo, B., Zhao, D., Sun, W., ... Zang, Q. (2022). Investigation of pore-throat structure and fractal characteristics of tight sandstones using HPMT, CRMI, and NMR methods: A case study of the lower Shihezi Formation in the Sulige area, Ordos Basin. *Journal of Petroleum Science and Engineering*, 210, 110053.
- Zang, Q., Liu, C., Awan, R. S., Yang, X., Lu, Z., Li, G., ... Ran, Y. (2022). Comparison of pore size distribution, heterogeneity and occurrence characteristics of movable fluids of tight oil reservoirs formed in different sedimentary environments: A case study of the Chang 7 member of Ordos Basin, China. *Natural Resources Research*, 31(1), 415–442.
- Zhao, H., Ning, Z., Zhao, T., Zhang, R., & Wang, Q. (2016). Effects of mineralogy on petrophysical properties and permeability estimation of the Upper Triassic Yanchang tight oil sandstones in Ordos Basin, northern China. *Fuel*, 186, 328–338.
- Zhao, J. Y., Luo, J. L., Lei, X. L., Guo, D. Y., & Xia, H. P. (2007). Provenance analysis of the sixth member of the Yanchang Formation in the Yangjiayuanze oil prospect area, Zichang oilfield, Ordos basin. *Geology in China*, 34(3), 422–429.
- Zhao, J. Z., Wu, S. B., & Wu, F. L. (2007). The classification and evaluation criterion of low permeability reservoir: An example from Ordos Basin. *Lithologic Reservoirs*, 19(3), 28–31.
- Zhu, H., Zhang, T., Zhong, D., Li, Y., Zhang, J., & Chen, X. (2019). Binary pore structure characteristics of tight sandstone reservoirs. *Petroleum Exploration and Development*, 46(6), 1297–1306.
- Zhu, R. K., Wu, S. T., Su, L., Cui, J. W., Mao, Z. G., & Zhang, X. X. (2016). Problems and future works of porous texture characterization of tight reservoirs in China. *Acta Petrolei Sinica*, 37(11), 1323–1336.
- Zou, C., Yang, Z., Zhang, G., Hou, L., Zhu, R., Tao, S., ... Wang, L. (2014). Conventional and unconventional petroleum “orderly accumulation”: Concept and practical significance. *Petroleum Exploration and Development*, 41(1), 14–30.

How to cite this article: Li, G., Liu, C., Zhou, Y., Wu, H., Awan, R. S., Shi, F., Wu, Y., Zang, Q., & Wu, Y. (2023). Controlling effects of pore-throat structure and fractal characteristics on the physical properties of ultra-low permeability sandstone reservoirs: A case study of the sixth member of the Yanchang Formation in the Xiaojiache area, Ordos Basin. *Geological Journal*, 58(5), 1945–1964. <https://doi.org/10.1002/gj.4700>